Title page

House dust mite drives pro-inflammatory eicosanoid reprogramming and macrophage effector functions

House dust mite reprograms eicosanoid metabolism

Fiona D. R. Henkel*, MSc.,[1] Antonie Friedl*, MSc.,[1] Mark Haid, Dipl. Biol.,[2] Dominique Thomas, PhD,[3] Tiffany Bouchery, PhD,[4,5] Pascal Haimerl, MSc.,[1] Marta de los Reyes Jiménez, Lic,[1] Francesca Alessandrini, PhD,[1] Carsten B. Schmidt-Weber, PhD,[1] Nicola L. Harris, PhD,[4,5] Jerzy Adamski, PhD,[2,6] Julia Esser-von Bieren, PhD[1]

*these authors contributed equally

Affiliations

[1]Center of Allergy and Environment (ZAUM), Technical University of Munich and Helmholtz Center Munich, 80802 Munich, Germany, member of the German Center for Lung Research

[2]Institute of Experimental Genetics, Genome Analysis Center, 85764 Neuherberg, Germany

[3]pharmazentrum frankfurt/ZAFES, Institute of Clinical Pharmacology, Goethe University Frankfurt, 60590 Frankfurt, Germany

[4]Laboratory of Intestinal Immunology, Global Health Institute, School of Life Sciences, École Polytechnique Fédérale de Lausanne (EPFL), 1015 Lausanne, Switzerland

[5]Department of Immunology and Pathology, Monash University, Central Clinical School, Alfred Medical Research and Education Precinct, Clayton VIC 3800, Australia

[6]Lehrstuhl für Experimentelle Genetik, Technische Universität München, 85350 Freising-Weihenstephan, Germany

Corresponding author

Julia Esser-von Bieren

Center of Allergy and Environment (ZAUM)

Technische Universität München and Helmholtz Zentrum München

80802 Munich

Germany

Telephone: +49 89 4140 3464
FAX: +49 89 4140 3452
E-mail: Julia.esser@tum.de

Declaration of all sources of funding: This study was supported by the German Research Foundation (DFG) (grants ES 471/2-1 and ES 471/3-1) and by the Else Kröner-Fresenius-Stiftung (grant 2015_A195). CSW receives grant support by the German Center for Lung Research (DZL; 82DZL00302). MH was supported by Innovative Medicines Initiative Joint Undertaking under Grant agreement number 115317 (DIRECT): "The work leading to this publication has received support from the Innovative Medicines Initiative Joint Undertaking under grant agreement n°115317 (DIRECT), resources of which are composed of financial contribution from the European Union's Seventh Framework Programme (FP7/2007-2013) and EFPIA companies' in kind contribution."

Conflicts of interest:
CSW received grant support from Allergopharma, PLS Design as well as Zeller AG and received speaker honoraria from Allergopharma. All authors have no conflict of interest in relation to this work.

ABSTRACT

Background
Eicosanoid lipid mediators play key roles in type 2 immune responses, e.g. in allergy and asthma. Macrophages represent major producers of eicosanoids and they are key effector cells of type 2 immunity. We aimed to comprehensively track eicosanoid profiles during type 2 immune responses to house dust mite (HDM) or helminth infection and to identify mechanisms and functions of eicosanoid reprogramming in human macrophages.

Methods
We established an LC-MS/MS workflow for the quantification of 52 oxylipins to analyze mediator profiles in human monocyte derived macrophages (MDM) stimulated with HDM and during allergic airway inflammation (AAI) or nematode infection in mice. Expression of eicosanoid enzymes was studied by qPCR and western blot and cytokine production was assessed by multiplex assays.

Results
Short (24h) exposure of alveolar-like MDM (aMDM) to HDM suppressed 5-LOX expression and product formation, while triggering prostanoid (thromboxane and prostaglandin D_2 and E_2) production. This eicosanoid reprogramming was p38-dependent, but Dectin-2-independent. HDM also induced pro-inflammatory cytokine production, but reduced granulocyte recruitment by aMDM. In contrast, high levels of cysteinyl leukotrienes (cysLTs) and 12-/15-LOX metabolites were produced in the airways during AAI or nematode infection in mice.

Conclusion
Our findings show that a short exposure to allergens as well as ongoing type 2 immune responses are characterized by a fundamental reprogramming of the lipid mediator metabolism with macrophages representing particularly plastic responder cells. Targeting mediator reprogramming in airway macrophages may represent a viable approach to prevent pathogenic lipid mediator profiles in allergy or asthma.

Word count: 3641

Key words
Eicosanoids; house dust mite; LC-MS/MS; macrophages; type 2 inflammation

Abbreviations:

5-LOX	5-lipoxygenase
COX	cyclooxygenase
cysLTs	cysteinyl leukotrienes
IS	internal standard
LTA_4H	leukotriene A_4 hydrolase
LTB_4	leukotriene B_4
LTC_4S	leukotriene C_4 synthase
LC-MS/MS	liquid chromatography tandem mass spectrometry
MDM	monocyte derived macrophages
PGs	prostaglandins
PMN	polymorphnuclear leukocytes
SPM	specialized pro-resolving mediator

INTRODUCTION

Lipid mediators govern immune responses in a multitude of infectious or chronic inflammatory settings (1). In allergy and asthma, prostanoids and leukotrienes (LTs) derived from the polyunsaturated fatty acid (PUFA) arachidonic acid (AA) drive hallmark type 2 immune responses such as eosinophil accumulation (2,3). AA metabolites (eicosanoids) have also been suggested to contribute to type 2 immunity during nematode infection (4–6). Despite these important immunological functions, few studies have comprehensively assessed lipid mediator profiles during type 2 immune responses. This is possibly due to the limited availability of adequate LC-MS/MS workflows, which are required for the simultaneous quantification of a multitude of structurally similar but functionally distinct mediators. Indeed, most immunological studies in allergy or nematode infection have used immunoassays to quantify less than a handful of mediators (5,7,8). However, LC-MS/MS analysis of 18 eicosanoids in macrophages from nematode infected mice suggested abundant and plastic eicosanoid production during type 2 immune responses (6). In addition, a number of studies have applied LC-MS/MS approaches to quantify up to 88 lipid mediators in *ex vivo* samples from allergy and asthma patients (9–12). Moreover, using macrophages as a model system, targeted lipidomics approaches were applied to quantify more than 100 eicosanoid metabolites (13). Due to their plasticity and abundant expression of eicosanoid biosynthetic pathways, macrophages present an attractive cellular model to study lipid mediator production in immunological settings (14). In the context of inflammasome activation, targeted lipidomics workflows allowed for the characterization of an “eicosanoid storm” during macrophage activation (15,16). However, despite these recent advances in lipidomics technologies, information about the lipid mediator profiles in type 2 immune responses remains scarce.

Here, we have established a targeted lipidomics workflow for the simultaneous quantification of 52 oxylipins from several PUFAs (AA, LA, DHA). We applied this workflow to demonstrate that HDM exposure of human macrophages results in a pronounced eicosanoid reprogramming, characterized by high levels of prostanoids (particularly thromboxane), but low levels of 5-LOX products. This eicosanoid reprogramming was dependent on p38 MAPK activation, but independent of Dectin-2. We further show that HDM-driven eicosanoid reprogramming occurs on the mRNA and

protein level and is associated with the production of pro-inflammatory cytokines and chemokines. However, HDM-exposed macrophages showed a reduced chemotactic potential towards granulocytes, correlating with suppressed LTB_4 production. Together, these findings suggest that HDM induces a pro-inflammatory macrophage phenotype with impaired effector function. Finally, we quantified mediator profiles in bronchoalveolar lavage fluid (BALF) from HDM-sensitized and nematode-infected mice, thus revealing profound changes in COX- and LOX metabolites during type 2 immune responses *in vivo*. In summary, these data show that the AA metabolism is fundamentally reprogrammed during type 2 immune responses and suggest macrophage reprogramming as an attractive target in type 2 inflammation.

MATERIALS AND METHODS

Animal experiments were performed according to institutional guidelines and to Swiss federal and cantonal laws on animal protection.

Material

Eicosanoids, PUFAs and deuterated internal standards (IS) were purchased from Cayman Chemical (Ann Arbour, MI, USA). An analyte and IS working solution was prepared as shown in Table S1/S2. LC-grade solvents (2-propanol, Carl Roth (Karlsruhe, Germany), acetonitrile, Thermo Fisher Scientific (Waltham, MA, USA), methanol, Applichem (Darmstadt, Germany)) and ultrapure H_2O (supplied through a MilliQ system (Merck Millipore, Darmstadt, Germany)) were used for mobile phase preparation.

Isolation and culture of polymorphnuclear leukocytes (PMN) and peripheral blood mononuclear Cells (PBMC)

Written informed consent in accordance with the Declaration of Helsinki was obtained from healthy volunteers before blood collection, which had been approved by the local ethics committee at the Technical University of Munich. PMN and PBMC were isolated and cultured in medium containing 10% heat-inactivated FBS and monocytes were differentiated to aMDM as described previously (17,18). Supernatants were stored at -80°C in 50% MeOH for LC-MS/MS or undiluted for cytokine analysis.

Chemotaxis Assay

PMN were incubated for 30 min at 37°C with pooled conditioned medium of aMDM ± HDM ± indomethacin (100µM, Cayman Chemical) ± DBM-1285. $2x10^5$ PMN were transferred to transwells (3µm pore size, Corning, NY, USA) and allowed to migrate for 3h at 37°C towards conditioned medium containing chemoattractants: 2 ng/ml LTB_4, Cayman Chemical; 20ng/ml IL-8; 2ng/ml CCL5, both Miltenyi Biotec. Migrated PMN were counted microscopically.

In vivo model of *N. brasiliensis* infection

Mice were infected subcutaneously with 200 larvae of *N. brasiliensis* (*Nb*), and BALF was collected on day 5 post infection as previously described (19,20).

In vivo model of HDM-induced allergic airway inflammation

C57BL/6J mice were sensitized by bilateral intranasal (i.n.) instillations of extract from *Dermatophagoides farinae* ("HDM") (1µg in 20µl PBS; Stallergenes). Challenges were performed on days 8-11 with 10µg HDM extract. Three days after the final challenge,

BALF (600µl) was collected, equal volumes of methanol were added and samples were frozen immediately at -80°C until further processing.

Real-Time PCR

aMDM were lysed in RLT Buffer (Qiagen, Hilden, Germany) with 1% β-Mercaptoethanol (Merck Millipore,), followed by RNA extraction (Zymo Research, Irvine, CA, USA) and reverse transcription according to the manufacturer's instructions (Thermo Fisher Scientific). qPCR analysis was performed as described previously (primers shown in Table S3) (18).

Western blotting

Western blotting was performed similarly to previously published procedures (18). A detailed procedure can be found in the supplement.

Multiplex Cytokine Assay and ELISA

Multiplex cytokine assays were performed as detailed in the supplement.

Sample Preparation for LC-MS/MS

Samples for method validation were prepared as triplicates in medium/MeOH (1:1) or PBS/MeOH (1:1) with an analyte concentration of 0.1, 1 or 10ng/ml (10x higher concentrations for PUFAs (Table S1/S2)). Automated solid phase extractions were performed with a Microlab STAR robot (Hamilton, Bonaduz, Switzerland). Prior to extraction all samples were diluted with H_2O to a MeOH content of 15% and 10µl of IS stock solution was added. Samples were extracted using Strata-X 96-well plates (30 mg, Phenomenex, Aschaffenburg, Germany) and eluted with MeOH. Samples were evaporated to dryness under N_2 stream and redissolved in 100µl MeOH/H_2O (1:1).

LC-MS/MS lipid mediator analysis

Chromatographic separation of eicosanoids was achieved with a 1260 Series HPLC (Agilent, Waldbronn, Germany) using a Kinetex C18 reversed phase column (2.6µm, 100 x 2.1mm, Phenomenex) with a SecurityGuard Ultra Cartridge C18 (Phenomenex) precolumn. The Sciex QTRAP 5500 mass spectrometer (Sciex, Darmstadt, Germany), equipped with a Turbo-V™ ion source, was operated in negative ionization mode. Identification of metabolites was achieved via retention time and scheduled multiple reaction monitoring (sMRM). Unique Q1/Q3 transitions were selected for each analyte by using single analyte injections and comparison with the literature (14). Analytes with identical MRM transitions were differentiated by retention time (Figure S1). A more detailed method description can be found in the supplement.

Data Analysis

All data were analyzed using GraphPad Prism 6 (GraphPad Software, La Jolla, CA, USA) or R 3.4.3 (21). For LC-MS/MS analysis all samples were normalized to their RNA content. Data were analyzed using Wilcoxon-, Friedman or Kruskal-Wallis test with respective post-hoc test as specified in the Figure legends and considered statistically significant if $p<0.05$.

RESULTS

Lipid mediators involved in type 2 immune responses can be detected with high accuracy, precision and recovery by LC-MS/MS

Quantification of lipid mediators in type 2 immune settings has resulted in discrepancies, depending on the analytical method (EIA or LC-MS/MS) (5,22). Thus, we compared these methods for leukotrienes, PGE_2 and TXB_2 in supernatants of human PMN and aMDM. Quantification by EIA showed higher variability, particularly for LTs: SD=8.48 (EIA) vs. SD=0.72 (LC-MS/MS) for LTB_4; SD=6.44 (EIA) vs. SD=0.23 (LC-MS/MS) for cysLTs. Levels obtained by EIA were also significantly higher as compared to LC-MS/MS and did not correspond well to AA-metabolizing enzymes (Figure 1A/ 4) (17).
Thus, we established an LC-MS/MS workflow for the comprehensive and simultaneous quantification of PUFA metabolites involved in type 2 inflammation (Figure 1B/S1, Tables S4-S9). At 1ng/ml we could detect 36 metabolites according to FDA guidelines (accuracy: ±15%, RSD <20%) (Table S4). This included eicosanoids (LTs, TXB_2, PGD_2) as well as specialized pro-resolving mediators (SPMs) (resolvin E1/D1 (RvE1/RvD1) and protectin D1 (PDX)) (Figure 1C/D, Table S4). The recovery ranged from 69-127% for key lipid mediators of type 2 inflammation with a matrix effect in a similar range (Figure 1E, Table S5). Thus, at concentrations ≥ 1ng/ml eicosanoid mediators of type 2 immunity (LTs, TXB_2, PGD_2) and several SPMs could be quantified with good accuracy, precision and recovery.

Zymosan exposure reprograms the eicosanoid metabolism of myeloid cells

In order to validate our LC-MS/MS workflow in a well-characterized cellular model, we processed and analyzed culture supernatants from human PMN that were either left untreated or exposed for 24h to zymosan prepared from fungal cell walls. First, a pool of PMN supernatants was measured in three technical replicates (Figure 2A-E) and second, levels of eicosanoids produced by PMN from different individuals (n=5) were analyzed separately (Figure 2F). Untreated PMN produced mainly 5-LOX metabolites (5-HETE and LTB_4) at a concentration of around 1.4 ng/ml and low levels of cysLTs (Figure 2A). PMN preparations contained neutrophils and eosinophils and thus had the capacity to generate LTs and 15-LOX metabolites (Figure 2A/B). Treatment with zymosan resulted in reprogramming of the eicosanoid metabolism, characterized by reduced production of LTB_4, cysLTs and 5-HETE (p=0.06) (Figure 2A/D/E/F). In contrast, zymosan exposure triggered the formation of COX-metabolites with a five-fold increase in TXB_2 levels. Additionally, zymosan-exposed PMN released PGE_2 and $PGF_2\alpha$ that were undetectable in unstimulated PMN (Figure 2C). Taken together, lipid mediator class-switching could be tracked by the developed LC-MS/MS workflow, allowing us to reveal previously reported as well as unprecedented zymosan-induced changes in the eicosanoid profile (23,24).

TGFβ1 induces a macrophage phenotype that resembles alveolar macrophages and resists IL-4 mediated regulation of eicosanoid pathways

Based on recent studies showing key roles for GM-CSF and TGFβ1 in alveolar macrophage (AM) differentiation (25,26) we differentiated human monocytes into alveolar-like macrophages (aMDM) and characterized their eicosanoid profile. At baseline, aMDM expressed high levels of 5-LOX and its respective oxylipin products (Figure 3A/4). In addition, aMDM expressed higher levels of 5-LOX and IL-1β as compared to MDM, suggesting that they adapted features of AM (Figure S2A/B) (27,28). IL-4 is known to reprogram the AA metabolism of macrophages by inducing 15-LOX, but suppressing 5-LOX and COX. We confirmed the IL-4-triggered induction of *ALOX15* in MDM from most donors during differentiation in the absence of TGFβ1 (Figure S2C). However, IL-4 had no significant impact on the eicosanoid profile of aMDM (Figure 3A-C), suggesting that aMDM resist IL-4-driven induction of 15-LOX as well as suppression

of COX and 5-LOX. Indeed, *PTGS2*, *PTGES*, *ALOX5*, and *ALOX15* mRNA levels remained unaffected by IL-4 (Figure 4A).

HDM exposure decreases 5-LOX- but increases COX metabolism in human alveolar-like macrophages via p38 MAPK

Next, we assessed the eicosanoid profile of aMDM during 24-96 h exposure to IL-4 and HDM. After 24h of HDM+IL-4 exposure, formation of 5-LOX products (LTB_4 and 5-HETE) was reduced (Figure 3A). Contrary to the effect on 5-LOX, HDM+IL-4 stimulation resulted in an increase of prostanoids (Figure 3B/S3A). In line with the LC-MS/MS data, 5-LOX mRNA levels were reduced by IL-4+HDM, while COX-2 was induced (Figure 4A). At later time points, we observed only minor changes in eicosanoid concentrations with the exception of PGD_2, which decreased after prolonged HDM exposure (Figure S3A), and 5-HETE and LTB_4, which initially decreased but increased back to control levels at 96h (Figure S3B/S3C).

In the absence of IL-4, HDM also triggered prostanoid production, while 5-LOX products were reduced in aMDM from 5 out of 7 donors (Figure 3D/E).

To identify the mechanisms underlying this eicosanoid reprogramming, we first neutralized Dectin-2, which has been described as the major C-type lectin receptor recognizing HDM (7). However, blocking Dectin-2 did not interfere with HDM-triggered changes in either COX or LOX metabolites (Figure 3F). Similarly, blockade of TLR-2 or TLR-4 or addition of polymyxin B to inactivate LPS did not affect mediator reprogramming by HDM (Figure S4). As the MAP kinase p38 has been implicated in the regulation of eicosanoid pathways (29), we assessed p38 phosphorylation in response to HDM. Levels of phosphorylated p38 were increased in HDM-exposed as compared to unstimulated aMDM and prostanoid formation was significantly reduced when macrophages were co-incubated with HDM and a p38 inhibitor (Figure 3F/G). In addition, p38 inhibition during HDM exposure restored 5-LOX product formation (Figure 3F, S5A).

We further examined the effect of HDM on mRNA and protein levels of COX and LOX pathway enzymes. *PTGES* (mPGES1) and *PTGS2* (COX-2) were increased, while *ALOX5* (5-LOX) expression was down-regulated by HDM on both transcript and protein level (Figure 4B/C). M2 polarization markers were either significantly reduced (*ALOX15*) or unaffected by HDM exposure (*TGM2*) (Figure 4A-C). Altogether, HDM-induced eicosanoid reprogramming likely occurred as a result of profound changes in the expression of eicosanoid pathway genes.

HDM exposure triggers the production of proinflammatory cytokines and chemokines

To study whether allergen-driven eicosanoid reprogramming was associated with an altered cytokine profile, we performed multiplex bead assays of supernatants from aMDM. We observed a significant increase in proinflammatory cytokines (IL-6, IL-1β, TNFα and IL-12 p70) after 24h HDM exposure (Figure 5A/B). HDM also triggered the release of chemokines (CXCL9/10, IL-8) involved in granulocyte recruitment (Figure 5A). Similar to the effects on eicosanoid reprogramming, p38 inhibition reduced the HDM-induced production of IL-6 and TNFα, while Dectin-2 neutralization did not affect the expression of these cytokines (Figure 5C/D, S5B).

HDM-exposed macrophages have a reduced capacity to recruit granulocytes

The recruitment of inflammatory neutrophils and eosinophils is a hallmark response of asthma. Thus, we addressed the functional consequence of HDM-driven mediator reprogramming by performing chemotaxis assays with human PMN. Migration of PMN

towards a chemoattractant mixture was diminished if PMN were exposed to supernatant from aMDM stimulated with HDM as compared to supernatant from unstimulated aMDM (Figure 5E). Addition of the COX inhibitor indomethacin during HDM stimulation did not affect the HDM-triggered reduction in chemotaxis, suggesting that prostanoids were not responsible for this effect. In contrast, p38 inhibition could restore PMN chemotaxis, correlating with increased LTB_4 levels (Figure S5A, S5C) and reduced IL-6, TNFα concentrations (Figure S5B).
Taken together, HDM-exposure induced a pro-inflammatory macrophage phenotype characterized by abundant production of bronchoconstrictive thromboxane and TNFα, but low production of LTB_4 and impaired chemotactic potential.

Distinct eicosanoid profiles are induced during the type 2 immune response to HDM or nematode infection in the airways

To assess whether eicosanoid reprogramming is a general feature of type 2 immune responses, we characterized lipid mediator profiles in the airways of HDM-sensitized or nematode-infected mice. When comparing eicosanoid profiles after sensitization and challenge with HDM or infection with the lung-migrating nematode *Nippostrongylus brasiliensis* (*Nb*), we observed an abundant formation of prostanoids in BALF from *Nb*-infected, but not from HDM-sensitized mice ($p < 0.05$ for all COX metabolites) (Figure 6A). In addition, no prostanoids could be detected in the BALF of naïve mice (Figure 6A). In contrast, cysLTs were detectable in the airways of *Nb*-infected as well as of HDM-sensitized mice (Figure 6B). Moreover, high levels of 12-/15-LOX metabolites (particularly 12-HETE and 13-HODE) were produced in the airways of *Nb*-infected and HDM-sensitized mice (Figure 6B/C). LA-derived metabolites (9-/13-HODE, 9,10-/11,13-DiHOME) were synthesized in similar quantities as compared to AA-metabolites in the airways after challenge with HDM or infection with *Nb* with a tendency for higher levels in *Nb*-infected mice ($p=0.025$ for 9,10 DiHOME, $p=0.124$ for 9-HODE). Finally, BALF from *Nb*-infected mice also contained detectable levels of SPMs (17-HDHA and RvD2) (Figure 6D). Thus, lipid mediator reprogramming occurs during the type 2 immune response to HDM or nematode parasites in the airways *in vivo* with partially distinct profiles. The induction of the COX- and simultaneous suppression of the 5-LOX pathway may represent an early response of macrophages in type 2 immune settings, which then governs the ensuing type 2 immune response to allergens or helminth infection.

DISCUSSION

Eicosanoid lipid mediators play central roles in type 2 immune responses, particularly in allergic inflammation. Thus, the comprehensive assessment of eicosanoid profiles in settings of type 2 inflammation can provide important information about the ensuing immune response and the functional plasticity of the cell types involved. Here, we describe an LC-MS/MS workflow, which allowed us to characterize eicosanoid reprogramming in two distinct settings of type 2 inflammation. First, we show that the lipid mediator metabolism of human alveolar-like macrophages (aMDM) is highly responsive to allergen-driven reprogramming. Second, we describe profound changes in lipid mediator profiles during the type 2 immune response to HDM or nematode infection *in vivo*.
Using a newly developed LC-MS/MS workflow, up to 52 oxylipins could be quantified in cell culture supernatants and biological samples from the airways. To our knowledge, this represents one of the largest oxylipin panels that has been validated and applied in the context of type 2 immune responses. This workflow, allowed for the sensitive and reliable quantification of central eicosanoid mediators of type 2 inflammation (e.g. LTs, TXB_2, PGD_2), whilst the accuracy should be improved for other mediators (e.g. PGE_2).

To initially validate the LC-MS/MS workflow, we studied zymosan-triggered eicosanoid reprogramming in human PMN. At baseline, stimulation with Ca^{2+} ionophore resulted in the release of 5-HETE and LTs, which is consistent with previous studies (30,31). In keeping with the literature, zymosan induced a shift in the eicosanoid metabolism, characterized by higher amounts of prostanoids (32). Previous studies largely focused on the acute effects of zymosan or HDM and showed that both stimuli could trigger LT production by myeloid cells, when applied for short times (2-60 min) (7,33). Here, we focused on the prolonged exposure to TLR2/ Dectin ligands (zymosan and HDM) as they are involved in the initiation of type 2 inflammation (2,8,34). Lipid mediator class-switching from 5-LOX to COX metabolites occurred for both stimuli, thus suggesting that lipid mediator reprogramming during type 2 inflammation happens analogous to settings of type 1 inflammation (16).

The induction of prostanoids and suppression of 5-LOX metabolites appears to be a common feature of macrophages in type 2 immune settings in response to allergens, IL-4 or nematode infection. Indeed, the reduced production of 5-LOX metabolites could be a result of high levels of IL-4 produced by T_H2 cells, ILC2s and/ or basophils (35) as IL-4 is known to suppress 5-LOX expression in various cell types, including macrophages (17,36). In a model of filarial nematode infection, eicosanoid reprogramming in nematode-elicited macrophages was shown to depend on IL-4 receptor signaling (6). In line with this study, we confirmed the induction of prostanoids for ~~two~~ a different nematode parasite~~s~~, thus suggesting that activation of the COX pathway is a general feature of the immune response to nematodes. Recently, soluble egg antigen of a distinct helminth species (the trematode *Schistosoma mansoni*) was reported to induce PGE_2, which contributed to T_H2 polarization (37). This suggests an important functional role of prostanoids during the type 2 immune response to helminth infection.

The plasticity of macrophages and their extraordinary capacity to produce lipid mediators suggests that these cells are key drivers of eicosanoid reprogramming in type 2 immunity. During allergen-triggered type 2 immune responses in the airways, the macrophage pool consists of resident alveolar macrophages (AMs) and macrophages derived from recruited monocytes (38). We used aMDM (differentiated in the presence of GM-CSF and TGFβ1) as a cellular model to mimic this mixed macrophage population. Although aMDM may not fully recapitulate macrophages in the lung, these cells showed several typical features of AMs, including high baseline expression of LT-biosynthetic enzymes and of the pro-inflammatory cytokine IL-1β (27,28).

We particularly focused on HDM extract as a trigger of type 2 inflammation with well-established functional roles for lipid mediators (2,8,39). Exposure of aMDM to HDM for 24-96h resulted in a dynamic mediator class switching of LOX and COX metabolites. While the production of regulatory mediators (e.g. PGE_2) peaked after 48h of HDM exposure, pro-inflammatory 5-LOX metabolites were initially suppressed, but increased back to baseline over time. This may explain why cysLTs were formed in the airways of HDM-sensitized mice during a two-week model of allergic airway inflammation. However, in addition to macrophages, other cell types including eosinophils and airway epithelial cells can contribute to the formation of LOX metabolites (including 5-LOX-derived cysLTs and 12/15-LOX derived HETEs and HODEs) during HDM-triggered airway inflammation *in vivo* (18). Nevertheless, macrophages likely represent a major source of lipid mediators during the initial exposure to HDM as they are abundant in the airways and highly express or readily upregulate LOX and COX enzymes.

Given the production of several neutrophil-chemotactic factors by HDM-exposed aMDM, we hypothesized that aMDM would show an increased potential to trigger granulocyte chemotaxis after HDM exposure. However, in line with previous *in vivo* studies, secretions from HDM-exposed aMDM rather tended to decrease granulocyte chemotaxis

(40). This may result in impaired host defense and thus increased susceptibility to infections, which is a common complication in asthmatic patients (41). To address the functional contribution of COX metabolites, we studied granulocyte chemotaxis in the presence of secretions from HDM-exposed aMDM, which had been treated with the COX inhibitor indomethacin. However, COX inhibition did not affect the chemotactic potential of HDM-exposed aMDM. Instead, a p38 inhibitor restored LTB_4 production and neutrophil chemotaxis, suggesting that the reduced production of the neutrophil chemoattractant LTB_4 by HDM-exposed aMDM may contribute to the impaired chemotactic potential.

Contrary to previous reports of Dectin-2 as an essential HDM receptor (7,8), we did not observe a reduction of HDM-triggered prostanoid or cytokine production when neutralizing Dectin-2. However, this may be due to the timing of Dectin-2 ligation as previous studies were focused on acute responses (20-60 minutes) after HDM exposure. Indeed, while the initial response might depend on Dectin-2, other mechanisms likely drive mediator reprogramming during longer exposure. Our results suggest that p38 activation by a Dectin-2 and TLR-2/-4-independent mechanism contributed to eicosanoid and cytokine reprogramming in macrophages.

Taken together, HDM exposure induced a potentially pathogenic macrophage phenotype, characterized by abundant production of prostanoids (particularly TXB_2) and pro-inflammatory cytokines (particularly TNFα). Given that several of the HDM-triggered macrophage mediators are implicated in severe, steroid-resistant airway inflammation, mediator reprogramming in macrophages should be explored as a therapeutic target in therapy-resistant allergy and asthma.

FIGURE LEGENDS

Figure 1. Lipid mediators involved in type 2 immune responses can be detected with high accuracy, precision and recovery by LC-MS/MS.
A Levels of major bioactive eicosanoids (mean + SD) in supernatants from PMN (n=5) or MDM (n=11-30) quantified by EIA or LC-MS/MS; **B** Sample preparation workflow; **C** Accuracy (%) at three different concentrations for key eicosanoids, shown as mean + SD. Dotted lines: ± 15% range; **D** Precision calculated as relative standard deviation (RSD) (%), shown as mean. Dotted lines: 15% and 20% RSD; **E** Recovery at 1 ng/ml. Dotted lines: ± 15% range. Samples in C-E were extracted and measured in triplicates on the same day. Statistical significance was determined using Wilcoxon test.

Figure 2. Zymosan triggers eicosanoid reprogramming in human granulocytes.
A Heatmap of LC-MS/MS data for human PMN (pool of n=6 donors) ± zymosan, analyzed as three technical replicates. **B** Neutrophil (left) or eosinophils (right) stained for 5-LOX and LTA4H or LTC4S and 15-LOX, respectively. Blue: DAPI (nuclei). **C**-**E** Levels of COX metabolites (C), leukotrienes (D) and HETEs (E) produced by PMN, presented as mean + SD (pool of n=6, measured in triplicates). **F** Levels of prostaglandins, leukotrienes and HETEs produced after 24h ± zymosan (n=5). Statistical significance was determined using Wilcoxon test.

Figure 3. House dust mite extract triggers COX- but suppresses 5-LOX metabolism in human alveolar-like macrophages via p38 MAPK.
A-**C** LC-MS/MS data for 5-LOX (A), COX (B), or 15-LOX (C) metabolites of aMDM, stimulated or not with 10ng/ml IL-4 ± 10µg/ml HDM (n=4); **D-F** LC-MS/MS data for COX

(D) or 5/15-LOX metabolites (E), (n=7) and of aMDM pre-incubated with p38 inhibitor or Dectin-2 neutralizing antibody (F) before HDM exposure (n=5). **G** Representative WB for total and phosphorylated p38 in aMDM (n=3). Data are shown as mean + SD; statistical significance was determined using Kruskal-Wallis test with Dunn's correction (A-C, F) or Wilcoxon test (D).

Figure 4. HDM-driven eicosanoid reprogramming occurs on the mRNA and protein level.
A and **B** relative gene expression of aMDM stimulated or not with 10ng/ml IL-4 ± 10 µg/ml HDM, (n=7) (A) or with 10µg/ml HDM (n=9) (B) for 24 h; **C** protein levels normalized to β-actin (upper panels) and representative WB images (lower panels) of aMDM ± 10µg/ml HDM for 24h (n=5-7). Data are shown as mean + SD; Statistical significance was determined using Wilcoxon test.

Figure 5. HDM exposure triggers the production of pro-inflammatory cytokines and chemokines, but reduces the granulocyte-chemotactic potential of human macrophages.
A Overview of cytokine levels [ng/ml], **B** TNFα, IL-12 p70 and IL-27 (mean + SD) for aMDM from 10 different blood donors ± 10µg/ml HDM for 24h; **C** concentration (n=10) and **D** gene expression (n=6) of IL-6 and TNFα in aMDM pre-incubated with p38 inhibitor VX702 or Dectin-2 neutralizing antibody before HDM exposure; **E** Percentage of granulocytes migrating towards supernatants (SN) of aMDM ± 10µg/ml HDM ± 100µM indomethacin (n=7). Statistical significance was determined using Wilcoxon test (B-D) or Friedman test with Dunn's correction (E).

Figure 6. Distinct eicosanoid profiles are induced during the type 2 immune response to HDM or nematode infection in the airways.
A-D LC-MS/MS analysis of prostanoids (A), LOX-metabolites of AA (B), LA metabolites (C) and SPMs (D) in BALF from HDM-sensitized or *Nb*-infected mice (n=3-6), representative data from two independent experiments are presented as mean + SD. Dotted lines represent levels for naïve mice. Statistical significance was determined using Kruskal-Wallis test with Dunn's correction

REFERENCES

1. Esser-von Bieren J. Immune-regulation and -functions of eicosanoid lipid mediators. *Biol Chem* 2017;**398**:1177–1191.

2. Barrett NA, Rahman OM, Fernandez JM, Parsons MW, Xing W, Austen KF et al. Dectin-2 mediates Th2 immunity through the generation of cysteinyl leukotrienes. *J Exp Med* 2011;**208**:593–604.

3. Hirai H, Tanaka K, Yoshie O, Ogawa K, Kenmotsu K, Takamori Y et al. Prostaglandin D2 selectively induces chemotaxis in T helper type 2 cells, eosinophils, and basophils via seven-transmembrane receptor CRTH2. *J Exp Med* 2001;**193**:255–261.

4. Machado ER, Ueta MT, Lourenço EV, Anibal FF, Sorgi CA, Soares EG et al. Leukotrienes play a role in the control of parasite burden in murine strongyloidiasis. *J Immunol Baltim Md 1950* 2005;**175**:3892–3899.

5. Patnode ML, Bando JK, Krummel MF, Locksley RM, Rosen SD. Leukotriene B4 amplifies eosinophil accumulation in response to nematodes. *J Exp Med* 2014;**211**:1281–1288.

6. Thomas GD, Rückerl D, Maskrey BH, Whitfield PD, Blaxter ML, Allen JE. The biology of nematode- and IL4Rα-dependent murine macrophage polarization in vivo as defined by RNA-Seq and targeted lipidomics. *Blood* 2012;**120**:e93–e104.

7. Barrett NA, Maekawa A, Rahman OM, Austen KF, Kanaoka Y. Dectin-2 Recognition of House Dust Mite Triggers Cysteinyl Leukotriene Generation by Dendritic Cells. *J Immunol* 2009;**182**:1119–1128.

8. Clarke DL, Davis NHE, Campion CL, Foster ML, Heasman SC, Lewis AR et al. Dectin-2 sensing of house dust mite is critical for the initiation of airway inflammation. *Mucosal Immunol* 2014;**7**:558–567.

9. Balgoma D, Larsson J, Rokach J, Lawson JA, Daham K, Dahlén B et al. Quantification of lipid mediator metabolites in human urine from asthma patients by electrospray ionization mass spectrometry: controlling matrix effects. *Anal Chem* 2013;**85**:7866–7874.

10. Kowal K, Gielicz A, Sanak M. The effect of allergen-induced bronchoconstriction on concentration of 5-oxo-ETE in exhaled breath condensate of house dust mite-allergic patients. *Clin Exp Allergy J Br Soc Allergy Clin Immunol* 2017;**47**:1253–1262.

11. Lundström SL, Yang J, Källberg HJ, Thunberg S, Gafvelin G, Haeggström JZ et al. Allergic asthmatics show divergent lipid mediator profiles from healthy controls both at baseline and following birch pollen provocation. *PloS One* 2012;**7**:e33780.

12. Mastalerz L, Celejewska-Wójcik N, Wójcik K, Gielicz A, Ćmiel A, Ignacak M et al. Induced sputum supernatant bioactive lipid mediators can identify subtypes of asthma. *Clin Exp Allergy J Br Soc Allergy Clin Immunol* 2015;**45**:1779–1789.

13. Dumlao DS, Buczynski MW, Norris PC, Harkewicz R, Dennis EA. High-throughput lipidomic analysis of fatty acid derived eicosanoids and N-acylethanolamines. *Biochim Biophys Acta* 2011;**1811**:724–736.

14. Norris PC, Dennis EA. A lipidomic perspective on inflammatory macrophage eicosanoid signaling. *Adv Biol Regul* 2014;**54**:99–110.

15. von Moltke J, Trinidad NJ, Moayeri M, Kintzer AF, Wang SB, van Rooijen N et al. Rapid induction of inflammatory lipid mediators by the inflammasome in vivo. *Nature* 2012;**490**:107–111.

16. Norris PC, Gosselin D, Reichart D, Glass CK, Dennis EA. Phospholipase A2 regulates eicosanoid class switching during inflammasome activation. *Proc Natl Acad Sci U S A* 2014;**111**:12746–12751.

17. Esser J, Gehrmann U, D'Alexandri FL, Hidalgo-Estévez AM, Wheelock CE, Scheynius A et al. Exosomes from human macrophages and dendritic cells contain enzymes for leukotriene biosynthesis and promote granulocyte migration. *J Allergy Clin Immunol* 2010;**126**:1032–1040, 1040.e1-4.

18. Dietz K, de Los Reyes Jiménez M, Gollwitzer ES, Chaker AM, Zissler UM, Rådmark OP et al. Age dictates a steroid-resistant cascade of Wnt5a, transglutaminase 2, and leukotrienes in inflamed airways. *J Allergy Clin Immunol* 2017;**139**:1343-1354.e6.

19. Bouchery T, Kyle R, Camberis M, Shepherd A, Filbey K, Smith A et al. ILC2s and T cells cooperate to ensure maintenance of M2 macrophages for lung immunity against hookworms. *Nat Commun* 2015;**6**:6970.

20. Camberis M, Le Gros G, Urban J Jr. Animal model of Nippostrongylus brasiliensis and Heligmosomoides polygyrus. *Curr Protoc Immunol Ed John E Coligan Al* 2003;**Chapter 19**:Unit 19.12.

21. R Core Team. *R: A Language and Environment for Statistical Computing*. Vienna, Austria: R Foundation for Statistical Computing 2017https://www.R-project.org/

22. Borgeat P, Fruteau de Laclos B, Rabinovitch H, Picard S, Braquet P, Hébert J et al. Eosinophil-rich human polymorphonuclear leukocyte preparations characteristically release leukotriene C4 on ionophore A23187 challenge. *J Allergy Clin Immunol* 1984;**74**:310–315.

23. Pouliot M, Gilbert C, Borgeat P, Poubelle PE, Bourgoin S, Créminon C et al. Expression and activity of prostaglandin endoperoxide synthase-2 in agonist-activated human neutrophils. *FASEB J Off Publ Fed Am Soc Exp Biol* 1998;**12**:1109–1123.

24. Esser J, Gehrmann U, Salvado MD, Wetterholm A, Haeggström JZ, Samuelsson B et al. Zymosan suppresses leukotriene C_4 synthase activity in differentiating monocytes: antagonism by aspirin and protein kinase inhibitors. *FASEB J Off Publ Fed Am Soc Exp Biol* 2011;**25**:1417–1427.

25. Yu X, Buttgereit A, Lelios I, Utz SG, Cansever D, Becher B et al. The Cytokine TGF-β Promotes the Development and Homeostasis of Alveolar Macrophages. *Immunity* 2017;**47**:903-912.e4.

26. Schneider C, Nobs SP, Kurrer M, Rehrauer H, Thiele C, Kopf M. Induction of the nuclear receptor PPAR-γ by the cytokine GM-CSF is critical for the differentiation of fetal monocytes into alveolar macrophages. *Nat Immunol* 2014;**15**:1026–1037.

27. Balter MS, Toews GB, Peters-Golden M. Different patterns of arachidonate metabolism in autologous human blood monocytes and alveolar macrophages. *J Immunol Baltim Md 1950* 1989;**142**:602–608.

28. Tomlinson GS, Booth H, Petit SJ, Potton E, Towers GJ, Miller RF et al. Adherent human alveolar macrophages exhibit a transient pro-inflammatory profile that confounds responses to innate immune stimulation. *PloS One* 2012;**7**:e40348.

29. Sokolowska M, Chen L-Y, Eberlein M, Martinez-Anton A, Liu Y, Alsaaty S et al. Low molecular weight hyaluronan activates cytosolic phospholipase A2α and eicosanoid production in monocytes and macrophages. *J Biol Chem* 2014;**289**:4470–4488.

30. Arm JP, Horton CE, House F, Clark TJH, Spur BW, Lee TH. Enhanced Generation of Leukotriene B_4 by Neutrophils Stimulated by Unopsonized Zymosan and by Calcium Ionophore after Exercise-induced Asthma. *Am Rev Respir Dis* 1988;**138**:47–53.

31. Gijón MA, Zarini S, Murphy RC. Biosynthesis of eicosanoids and transcellular metabolism of leukotrienes in murine bone marrow cells. *J Lipid Res* 2007;**48**:716–725.

32. Goldstein IM, Malmsten CL, Samuelsson B, Weissmann G. Prostaglandins, thromboxanes, and polymorphonuclear leukocytes: mediation and modulation of inflammation. *Inflammation* 1977;**2**:309–317.

33. Dalli J, Serhan CN. Specific lipid mediator signatures of human phagocytes: microparticles stimulate macrophage efferocytosis and pro-resolving mediators. *Blood* 2012;**120**:e60–e72.

34. Han M, Chung Y, Young Hong J, Rajput C, Lei J, Hinde JL et al. Toll-like receptor 2-expressing macrophages are required and sufficient for rhinovirus-induced airway inflammation. *J Allergy Clin Immunol* 2016;**138**:1619–1630.

35. Voehringer D, Shinkai K, Locksley RM. Type 2 immunity reflects orchestrated recruitment of cells committed to IL-4 production. *Immunity* 2004;**20**:267–277.

36. Spanbroek R, Hildner M, Köhler A, Müller A, Zintl F, Kühn H et al. IL-4 determines eicosanoid formation in dendritic cells by down-regulation of 5-lipoxygenase and up-regulation of 15-lipoxygenase 1 expression. *Proc Natl Acad Sci U S A* 2001;**98**:5152–5157.

37. Kaisar MMM, Ritter M, Del Fresno C, Jónasdóttir HS, van der Ham AJ, Pelgrom LR et al. Dectin-1/2-induced autocrine PGE2 signaling licenses dendritic cells to prime Th2 responses. *PLoS Biol* 2018;**16**:e2005504.

38. Zasłona Z, Przybranowski S, Wilke C, van Rooijen N, Teitz-Tennenbaum S, Osterholzer JJ et al. Resident alveolar macrophages suppress, whereas recruited monocytes promote, allergic lung inflammation in murine models of asthma. *J Immunol Baltim Md 1950* 2014;**193**:4245–4253.

39. Zasłona Z, Okunishi K, Bourdonnay E, Domingo-Gonzalez R, Moore BB, Lukacs NW et al. Prostaglandin E_2 suppresses allergic sensitization and lung inflammation by targeting the E prostanoid 2 receptor on T cells. *J Allergy Clin Immunol* 2014;**133**:379–387.

40. Habibzay M, Saldana JI, Goulding J, Lloyd CM, Hussell T. Altered regulation of Toll-like receptor responses impairs antibacterial immunity in the allergic lung. *Mucosal Immunol* 2012;**5**:524–534.

41. James KM, Peebles RS, Hartert TV. Response to infections in patients with asthma and atopic disease: an epiphenomenon or reflection of host susceptibility? *J Allergy Clin Immunol* 2012;**130**:343–351.

Author contributions:

Performed experiments: FDRH, AF, MH, DT, TF, PH, MRJ, FA; Analyzed data: FDRH, AF, MH, DT, JEvB; Designed the study: JEvB, JA, NLH, CBSW; Wrote the manuscript: JEvB, FDRH, AF.

Acknowledgements:
The authors wish to thank the animal care takers of the University of Lausanne for animal husbandry and Manuel Kulagin and Beatrice Volpe for technical assistance, as well as Carlo Angioni and Yannick Schreiber of University of Frankfurt for help with LC-MS/MS analysis. We would also like to thank Werner Römisch-Margl at the Helmholtz Zentrum München for setting up the Hamilton robot extraction method.

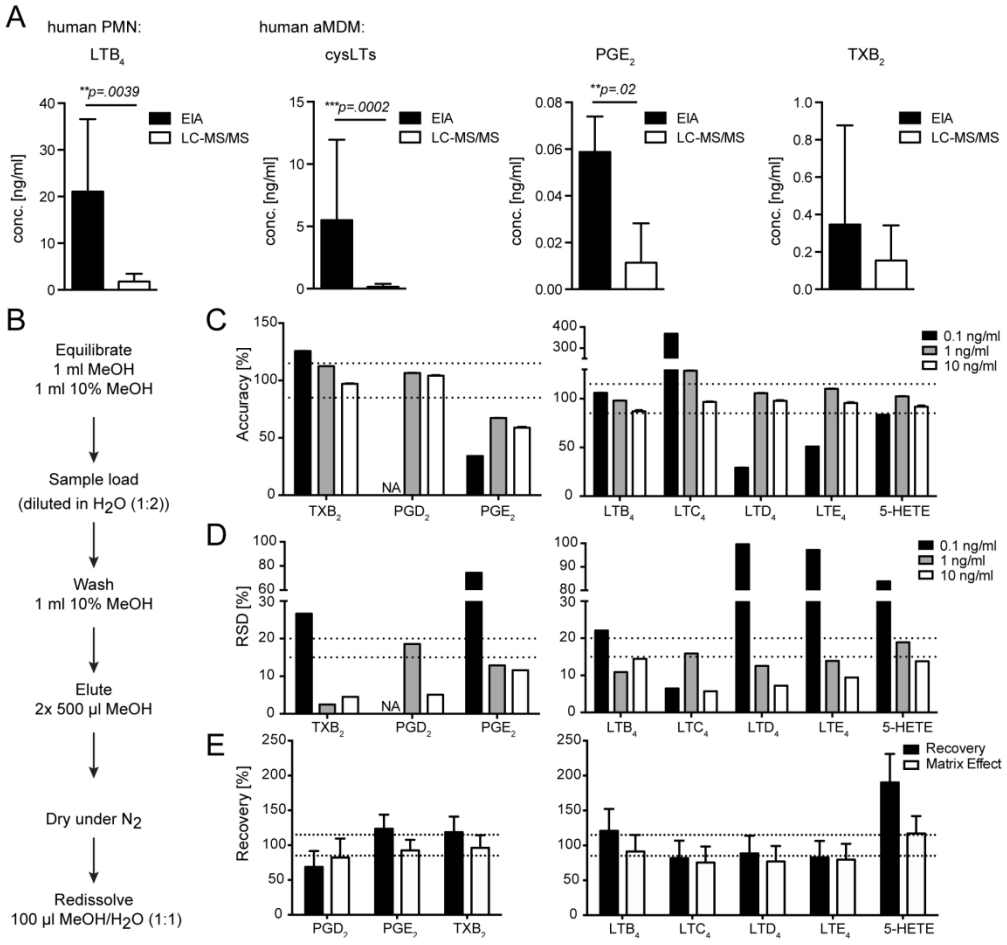

Figure 1. Lipid mediators involved in type 2 immune responses can be detected with high accuracy, precision and recovery by LC-MS/MS.

A Levels of major bioactive eicosanoids (mean + SD) in supernatants from PMN (n=5) or MDM (n=11-30) quantified by EIA or LC-MS/MS; B Sample preparation workflow; C Accuracy (%) at three different concentrations for key eicosanoids, shown as mean + SD. Dotted lines: ± 15% range; D Precision calculated as relative standard deviation (RSD) (%), shown as mean. Dotted lines: 15% and 20% RSD; E Recovery at 1 ng/ml. Dotted lines: ± 15% range. Samples in C-E were extracted and measured in triplicates on the same day. Statistical significance was determined using Wilcoxon test.

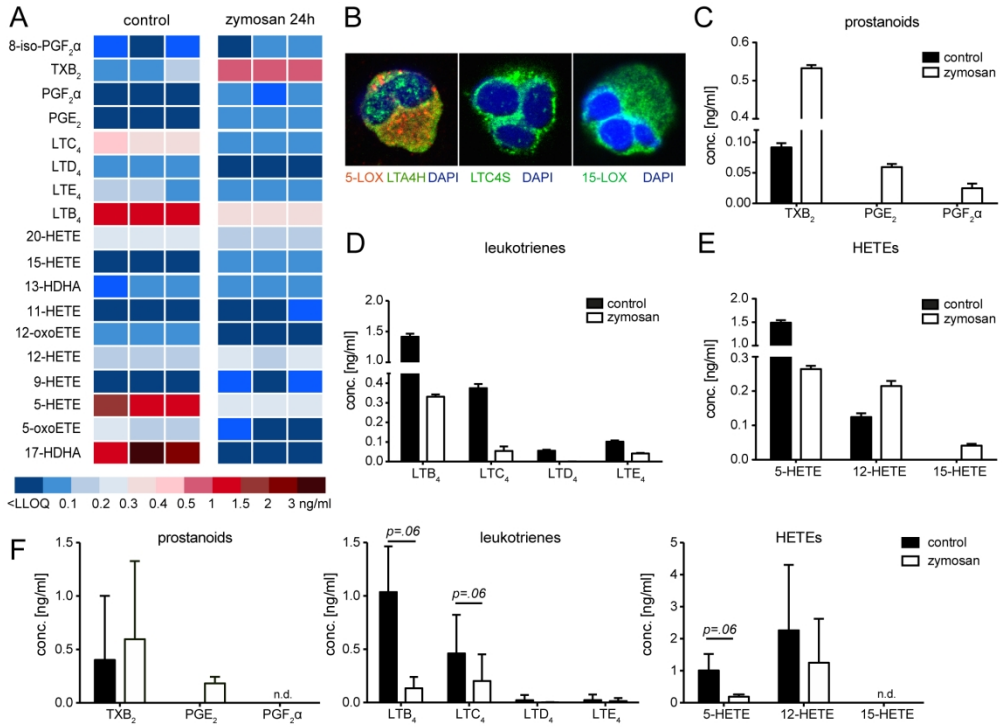

Figure 2. Zymosan triggers eicosanoid reprogramming in human granulocytes.
A Heatmap of LC-MS/MS data for human PMN (pool of n=6 donors) ± zymosan, analyzed as three technical replicates. B Neutrophil (left) or eosinophils (right) stained for 5-LOX and LTA4H or LTC4S and 15-LOX, respectively. Blue: DAPI (nuclei). C-E Levels of COX metabolites (C), leukotrienes (D) and HETEs (E) produced by PMN, presented as mean + SD (pool of n=6, measured in triplicates). F Levels of prostaglandins, leukotrienes and HETEs produced after 24h ± zymosan (n=5). Statistical significance was determined using Wilcoxon test.

186x138mm (300 x 300 DPI)

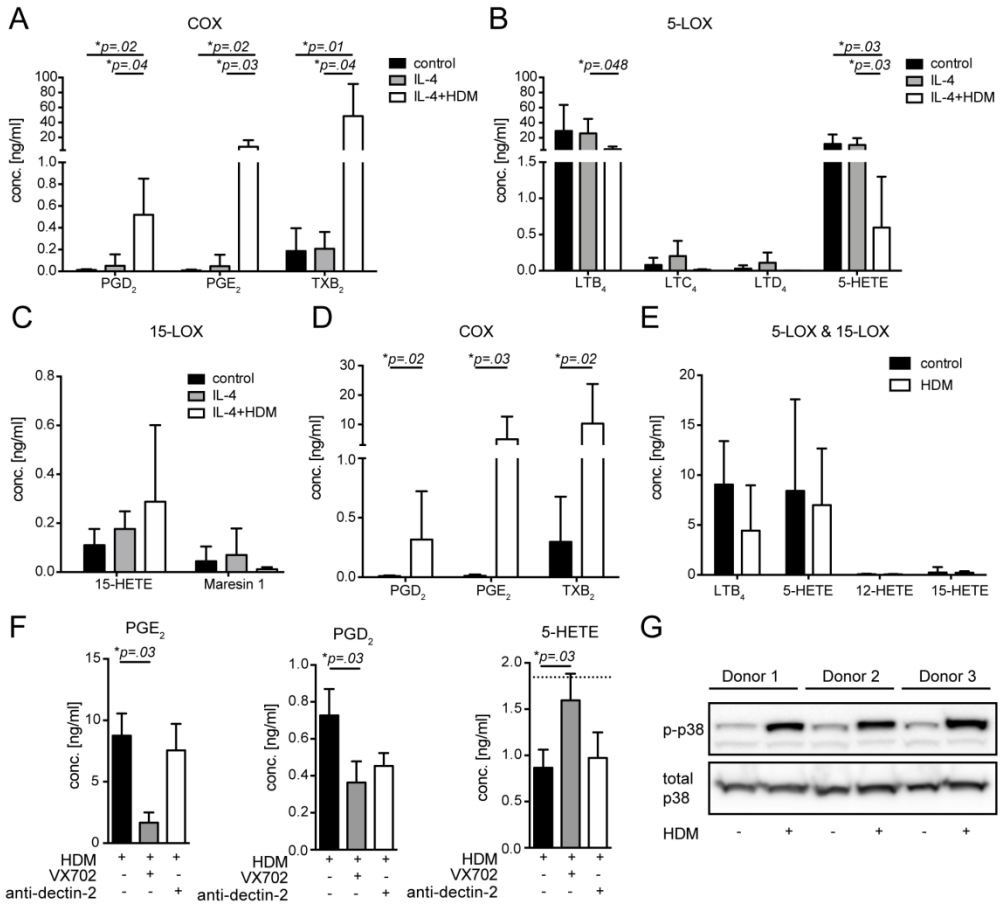

Figure 3. House dust mite extract triggers COX- but suppresses 5-LOX metabolism in human alveolar-like macrophages via p38 MAPK.

A-C LC-MS/MS data for 5-LOX (A), COX (B), or 15-LOX (C) metabolites of aMDM, stimulated or not with 10ng/ml IL-4 ± 10µg/ml HDM (n=4); D-F LC-MS/MS data for COX (D) or 5/15-LOX metabolites (E), (n=7) and of aMDM pre-incubated with p38 inhibitor or Dectin-2 neutralizing antibody (F) before HDM exposure (n=5). G Representative WB for total and phosphorylated p38 in aMDM (n=3). Data are shown as mean + SD; statistical significance was determined using Kruskal-Wallis test with Dunn's correction (A-C, F) or Wilcoxon test (D).

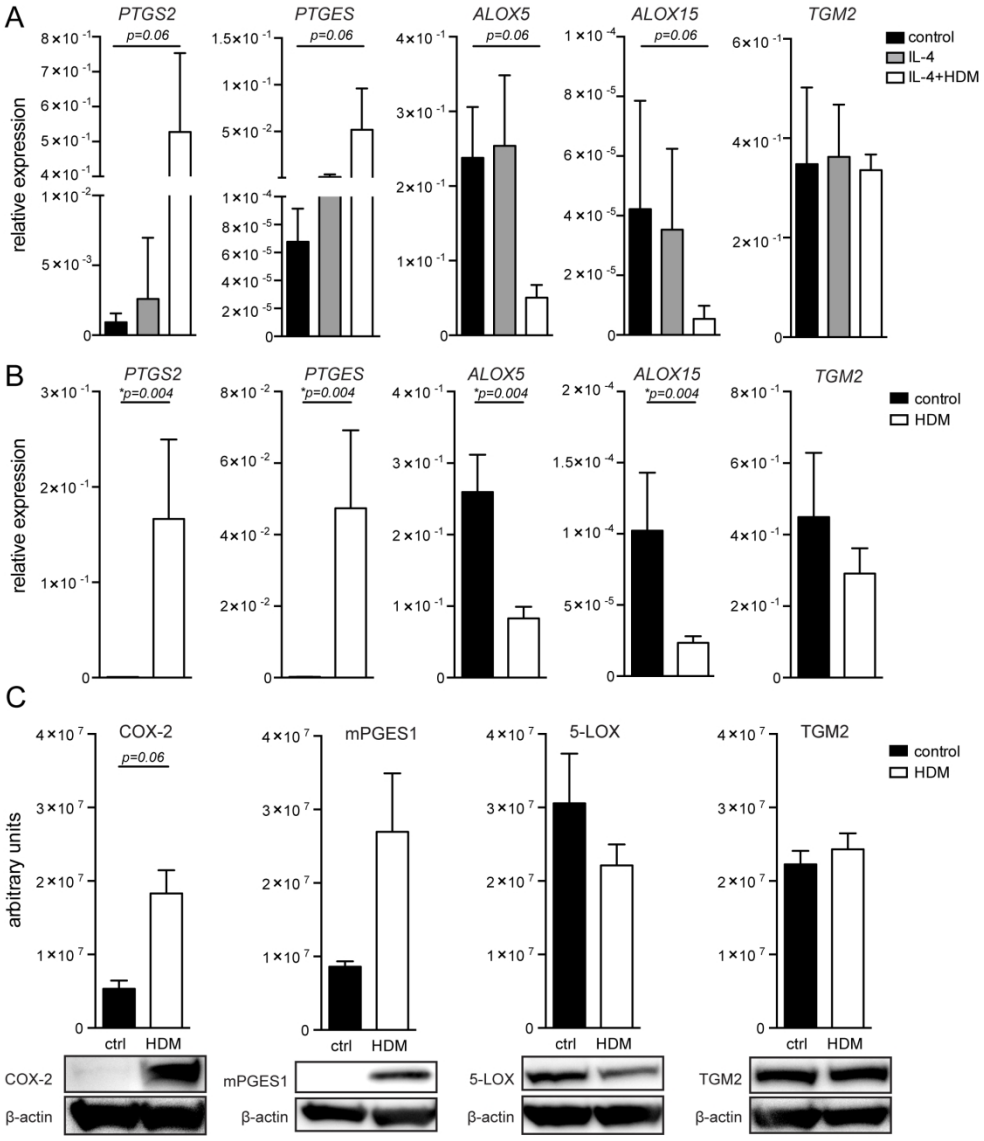

Figure 4. HDM-driven eicosanoid reprogramming occurs on the mRNA and protein level.
A and B relative gene expression of aMDM stimulated or not with 10ng/ml IL-4 ± 10 µg/ml HDM, (n=7) (A) or with 10µg/ml HDM (n=9) (B) for 24 h; C protein levels normalized to β-actin (upper panels) and representative WB images (lower panels) of aMDM ± 10µg/ml HDM for 24h (n=5-7). Data are shown as mean + SD; Statistical significance was determined using Wilcoxon test.

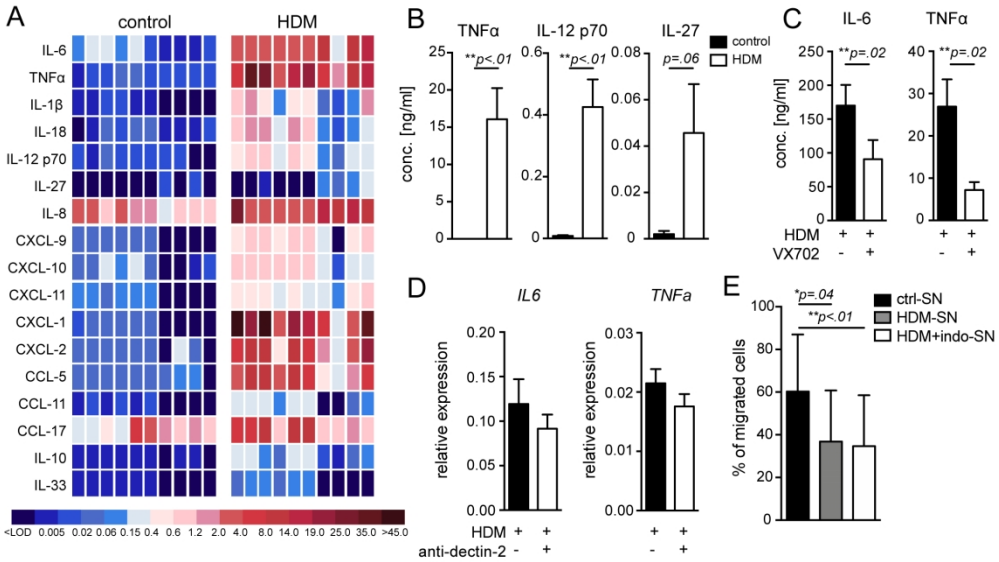

Figure 5. HDM exposure triggers the production of pro-inflammatory cytokines and chemokines, but reduces the granulocyte-chemotactic potential of human macrophages.
A Overview of cytokine levels [ng/ml], B TNFα, IL-12 p70 and IL-27 (mean + SD) for aMDM from 10 different blood donors ± 10µg/ml HDM for 24h; C concentration (n=10) and D gene expression (n=6) of IL-6 and TNFα in aMDM pre-incubated with p38 inhibitor VX702 or Dectin-2 neutralizing antibody before HDM exposure; E Percentage of granulocytes migrating towards supernatants (SN) of aMDM ± 10µg/ml HDM ± 100µM indomethacin (n=7). Statistical significance was determined using Wilcoxon test (B-D) or Friedman test with Dunn's correction (E).

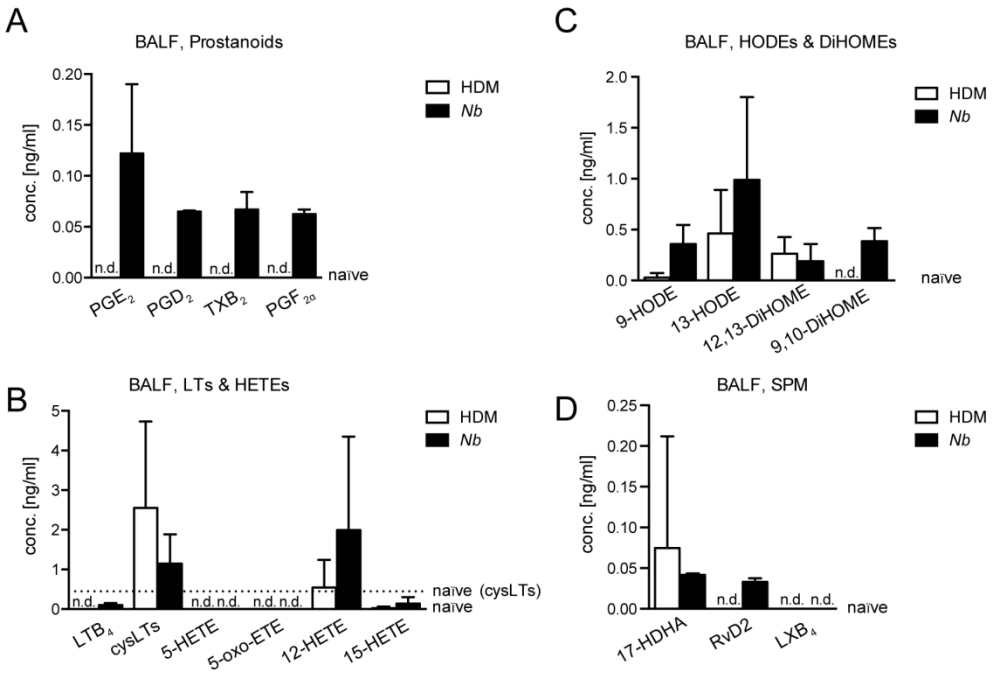

Figure 6. Distinct eicosanoid profiles are induced during the type 2 immune response to HDM or nematode infection in the airways.
A-D LC-MS/MS analysis of prostanoids (A), LOX-metabolites of AA (B), LA metabolites (C) and SPMs (D) in BALF from HDM-sensitized or Nb-infected mice (n=3-6), representative data from two independent experiments are presented as mean + SD. Dotted lines represent levels for naïve mice. Statistical significance was determined using Kruskal-Wallis test with Dunn's correction

157x106mm (300 x 300 DPI)

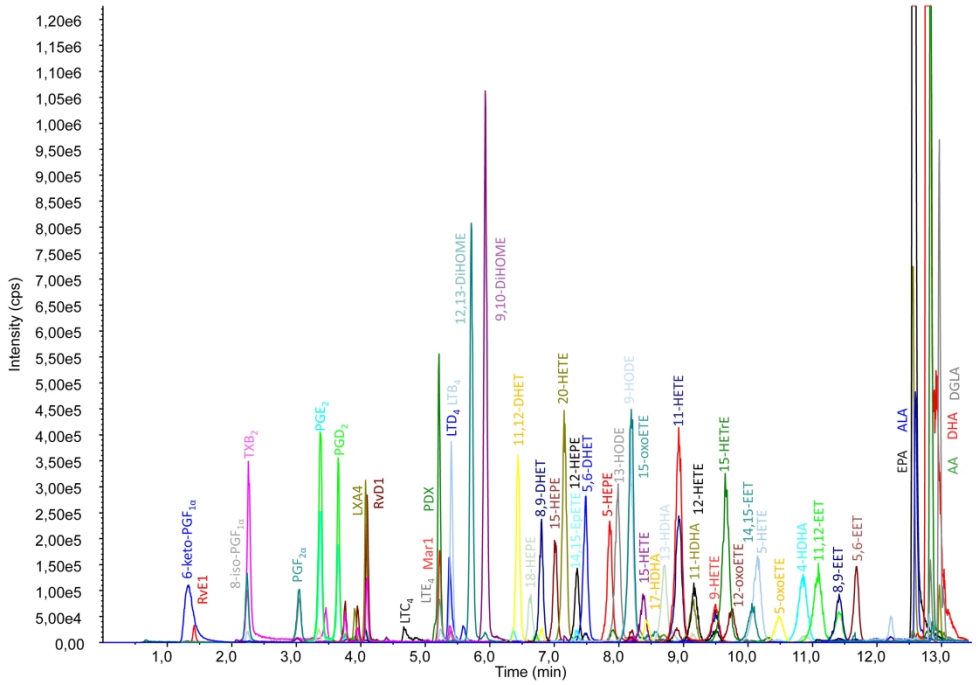

279x190mm (300 x 300 DPI)

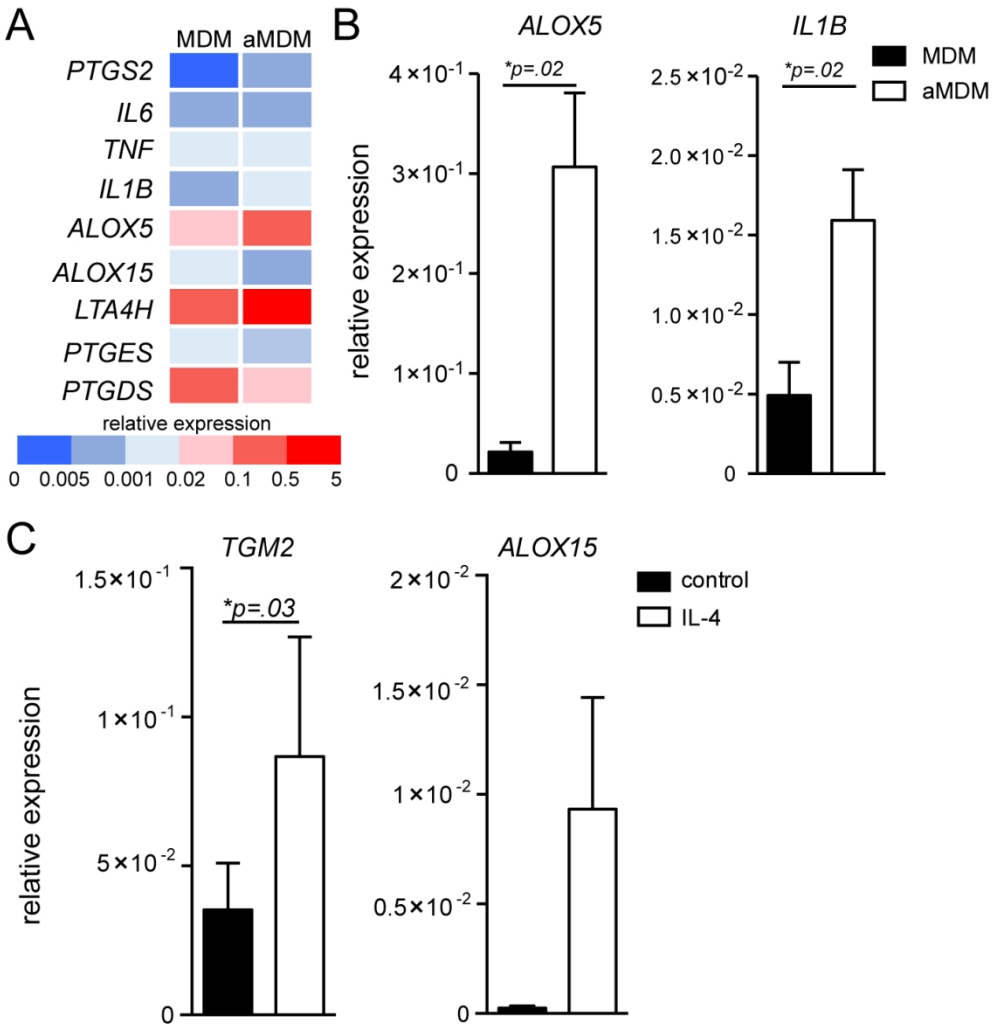

119x126mm (300 x 300 DPI)

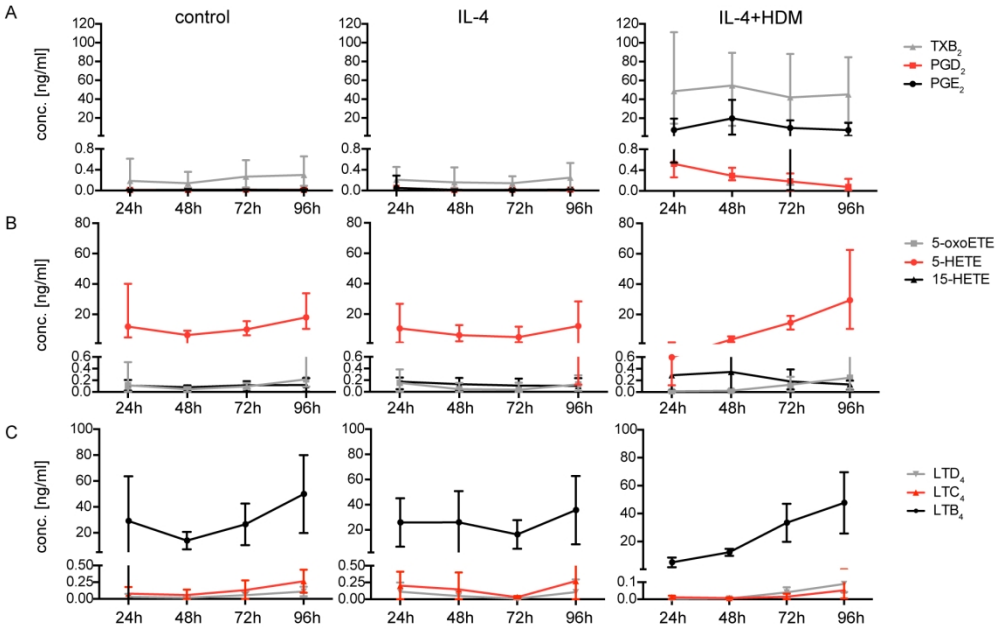
A
control
IL-4
IL-4+HDM
conc. [ng/ml]
TXB2
PGD2
PGE2
B
5-oxoETE
5-HETE
15-HETE
C
LTD4
LTC4
LTB4
24h
48h
72h
96h

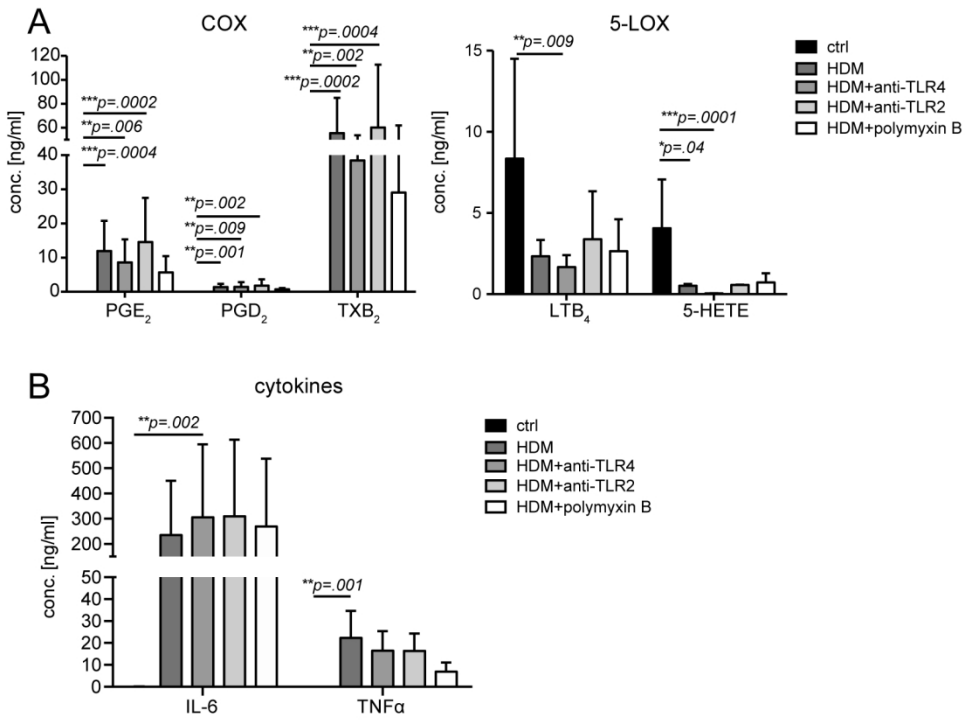
A
COX
5-LOX
conc. [ng/ml]
***p=.0002
**p=.006
***p=.0004
**p=.002
**p=.009
**p=.001
***p=.0004
**p=.002
***p=.0002
**p=.009
*p=.04
***p=.0001
PGE2
PGD2
TXB2
LTB4
5-HETE
ctrl
HDM
HDM+anti-TLR4
HDM+anti-TLR2
HDM+polymyxin B
B
cytokines
**p=.002
**p=.001
IL-6
TNFα

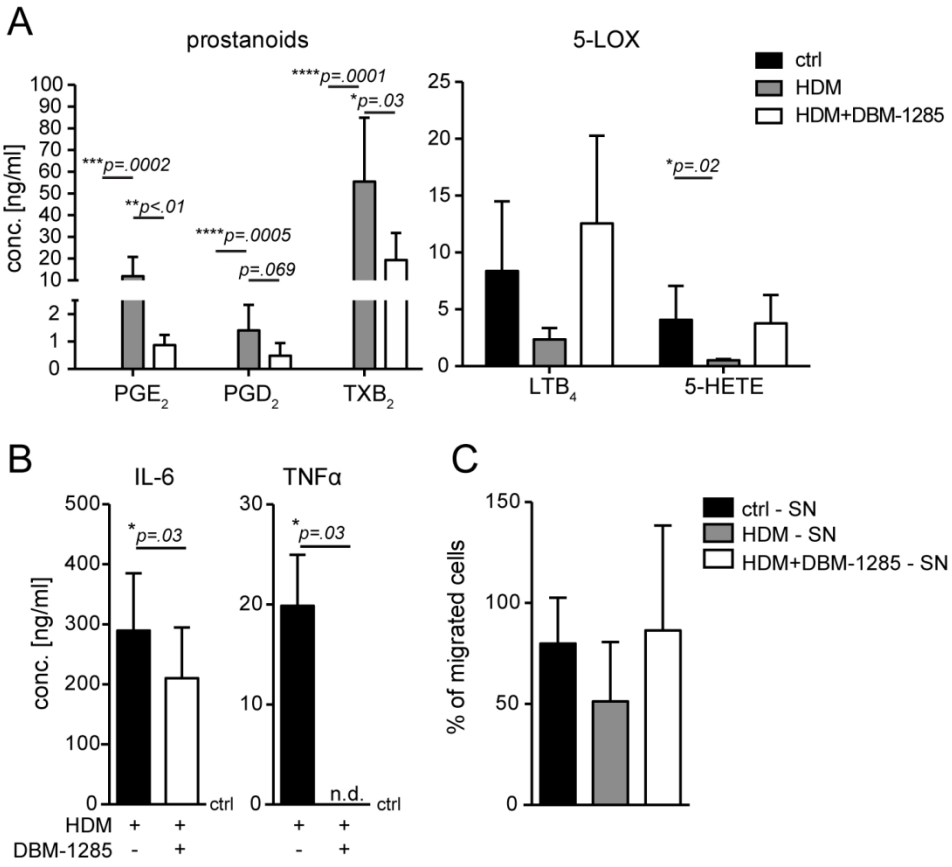
A
prostanoids
5-LOX
ctrl
HDM
HDM+DBM-1285
conc. [ng/ml]
***p=.0002
**p<.01
****p=.0005
p=.069
****p=.0001
*p=.03
*p=.02
PGE2
PGD2
TXB2
LTB4
5-HETE
B
IL-6
TNFα
*p=.03
*p=.03
conc. [ng/ml]
ctrl
n.d.
ctrl
HDM + + + +
DBM-1285 - + - +
C
ctrl - SN
HDM - SN
HDM+DBM-1285 - SN
% of migrated cells

House dust mite drives pro-inflammatory eicosanoid reprogramming and macrophage effector functions

House dust mite reprograms eicosanoid metabolism

Fiona D. R. Henkel*, MSc.,[1] Antonie Friedl*, MSc.,[1] Mark Haid, Dipl. Biol.,[2] Dominique Thomas, PhD,[3] Tiffany Bouchery, PhD,[4,5] Pascal Haimerl, MSc.,[1] Marta de los Reyes Jiménez, Lic,[1] Francesca Alessandrini, PhD,[1] Carsten B. Schmidt-Weber, PhD,[1] Nicola L Harris, PhD,[4,5] Jerzy Adamski, PhD,[2,6] Julia Esser-von Bieren, PhD[1]

*these authors contributed equally

Supplemental material

Methods

Isolation and culture of polymorphnuclear leukocytes (PMN) and peripheral blood mononuclear Cells (PBMC)

PMN and PBMC were isolated and cultured as previously described in medium containing 10 % heat-inactivated FBS (18,19). PMN were stimulated with 50 µg/ml zymosan (24h), followed by 5 µM Ca^{2+}-ionophore A23187 (10 min) (both Sigma Aldrich, Darmstadt, Germany). Monocytes were differentiated to aMDM as described previously (17,18). Cells were stimulated with *Dermatophagoides farinae* (HDM, 10 µg/ml, Stallergenes, Antony, France; LPS content: 549 EU/ml, determined by Pierce endotoxin quantification kit, Thermo Fisher Scientific), IL-4 (10 ng/ml, Miltenyi Biotec) or both for 24 h. A p38 inhibitor (VX-702, 1 µM, Cayman or DBM-1285 dihydrochloride, 1 µM, Tocris Bioscience, Bristol, UK), a Dectin-2-neutralizing antibody (10 µg/ml, Invivogen, Toulouse, France), anti-TLR2 (10 µg/ml, Invivogen) or anti-TLR4 antibody (10 µg/ml, Invivogen) was added 2h before or polymyxin B (5 µg/ml, Sigma Aldrich) concurrently with HDM stimulation. Before harvest aMDM were stimulated with Ca^{2+}-ionophore A23187 in the same manner as PMN. Supernatants were stored at -80°C in 50% MeOH for LC-MS/MS or undiluted for cytokine analysis.

Multiplex Cytokine Assay and ELISA

Multiplex cytokine assays (Magnetic Luminex Assay for Eotaxin (CCL11), GROα (CXCL1), GROβ (CXCL2), IL-1β, IL-18, IL-6, TARC (CCL17), IP-10 (CXCL10), IL-8 (CXCL8), IL-10, IL-27, TNFα, RANTES (CCL5), ITAC-1 (CXCL11), MIG (CXCL9), IL-12 p70, IL-33, R&D Systems, Minneapolis, MN, USA) were performed according to the manufacturer's instructions on a Bio Plex 200 System (Bio-Rad, Munich, Germany). ELISAs for human TNFα (R&D Systems) or IL-6 (BD Biosciences, San Diego, CA, USA) or eicosanoid EIAs (LTB_4, cysLTs, PGE_2, TXB_2; Cayman Chemical) were performed according to the manufacturers' instructions.

LC-MS/MS lipid mediator analysis

Lipid mediators were eluted with a gradient consisting of mobile phase A H_2O/acetonitrile/acetic acid (70:30:0.01, v/v/v) and mobile phase B 2-propanol. After 1 min of 100% A, the solvent was decreased to 33% within 1.5 min, held isocratic for 7.5 min. Over 2 min B was increased to 100% and held for 2.5 min. The flow-rate was set to 450 µl/min and reduced to 400 µl/min, when the gradient had reached 100% 2-propanol.

After every scheduled measurement, a 5 min clean-run was performed, ramping from acetonitrile/2-propanol (3:1) over 3.5 min to H_2O/acetonitrile/acetic acid (70:30:0.01, v/v/v), which was maintained for another 1.5 min, at an overall flow rate of 300 µl/min.
The column oven was operated at 40 °C. Samples (20 µl) were injected by an HTC PAL auto-sampler (CTC Analytics, Zwingen, Switzerland), set to 4 °C. Mass spectrometric parameters were set to: curtain gas 40 psi, ionspray voltage -4000 V, source temperature 500 °C, ion source gas 1 with 50 psi and ion source gas 2 with 40 psi. Declustering potential (DP), collision energy (CE), and cell exit potential (CXP) were optimized for each sMRM. sMRMs were measured within a 90 s time window.
The calibration curve for each analyte was obtained using an analyte stock solution at concentrations of 0.005, 0.01, 0.05, 0.1, 0.5, 1, 5, 10, and 50 ng/ml with constant levels of IS (1 ng/ml), prepared in medium/MeOH (1:1) and extracted as specified for the samples. Concentrations for PUFAs were 10x higher. The area under the curve of each metabolites was linked to its respective internal standard area to obtain the area ratio. Analyte individual calibration curves were obtained by plotting the area ratio against concentrations.
Acquisition of LC-MS/MS data was performed using Analyst Software 1.6.3 followed by quantification with MultiQuant Software 3.0.2 (both Sciex, Darmstadt, Germany).

Method Validation
To calculate the recovery for each metabolite, the analyte response of medium samples, medium:MeOH (1:1, v/v) spiked with analyte mix and extracted as a sample, was compared to not extracted samples, the same concentration of analyte mix spiked into MeOH:H_2O (1:1, v/v), without being extracted. The pure matrix effect was calculated as the ratio between the metabolite response in medium and the response in PBS (PBS:MeOH (1:1, v/v) spiked with analyte mix and extracted) extracted samples. Recovery and matrix effects for each analyte x were calculated as follows for each analyte:

$$Recovery\ (\%) = \frac{area\ ratio_{medium}\ (x)}{area\ ratio_{not\ extracted\ sample}\ (x)}$$

$$Matrix\ effect\ (\%)\ = \frac{area\ ratio_{medium}(x)}{area\ ratio_{PBS}\ (x)}$$

Accuracy and precision were determined by extracting the calibration curve 4-times. The accuracy was calculated as the ratio between the measured concentration in the samples and the theoretical concentration.

$$Accuracy\ (\%) = \frac{Concentration\ measured(x)}{Concentration\ spiked(x)}$$

The precision, estimating the variance of the extraction, was calculated as the relative standard deviation (RSD):

$$RSD\ (\%)\ = \frac{sd_c(x)}{mean_c(x)}$$

The limit of detection (LOD), the smallest concentration that can be distinguished from zero, was determined as signal to noise ratio (S/N) > 3 and the lower limit of quantification (LLOQ) was defined by a precision <20% of the quadruplicate calibration curve.

Stability
The analyte stability at 4 °C was obtained by consecutive measurements after 24 h and 48 h of the same sample, left in the autosampler. The reproducibility of the measurement was assessed by comparing calibration curves for extracted samples analyzed on three different days.

Linearity
The linearity of the method for each analyte was determined by calculating the Pearson correlation coefficient (R-value) of the calibration curve. R-values of all analytes were greater than 0.995.

Inter-day variability
Inter-day precision and accuracy were assessed on three consecutive days. Precision varied between 2% and 61% at 0.1 ng/ml, while at higher concentrations only 2 metabolites showed an RSD >20%. Inter-day accuracy varied between 85% - 230% over all concentration levels.

Tables (legends see below)

1) Analyte stock solutions with MRM parameters
2) Internal standard stock solution with MRM parameters
3) Primers for qPCR
4) Intraday accuracy and precision (RSD)
5) Recovery and Matrix Effect
6) 48 h Stability at 4 °C
7) Interday variability of precision and accuracy
8) LOD/LOQ + Linearity
9) LC-MS/MS data comparison ("Frankfurt vs. Munich panel")

Western blotting
Cells were lysed in RIPA buffer (Thermo Scientific, Waltham, MA, USA) supplemented with protease inhibitor (cOmplete tablets EDTA free, EASYpack, Roche Diagnostics, Mannheim, Germany) and phosphatase inhibitor (PhosSTOP tablets, EASYpack, Roche Diagnostics) in concentrations as indicated by the manufacturer. Protein concentration was assessed by Pierce BCA Protein Assay kit (Thermo Fisher Scientific) and lysates diluted to equal concentrations in deionized H_2O. Samples were heated under reducing conditions and run on Bolt 4-12% Bis-Tris Plus 12-well gels (Invitrogen, Thermo Fisher Scientific) for 60 minutes with constant voltage at 125 V using a Mini Gel Tank system (GE Healthcare Life Technologies, Freiburg, Germany). Western blotting was performed on an Immobilon-P Transfer membrane (Merck Chemical, Darmstadt, Germany) followed by blocking in 5% nonfat milk (AppliChem, Darmstadt, Germany) in TRIS-buffered saline with 0.5% Tween-20 (TBS-T, EMD Millipore, Billerica, MA, USA). Primary antibodies (goat-anti-COX2: Cayman Chemical, Ann Arbor, MI, USA, rabbit-anti-5-LOX, a kind gift or Dr. Olof P. Rådmark, Karolinska Institutet, Stockholm, Sweden rabbit-anti-TGM2: Cell Signaling, Danvers, MA, USA, mouse-anti-β-actin: Sigma Aldrich, Darmstadt. Germany) were diluted in 5% non-fat milk and membranes were incubated overnight. After washing in TBS-T, membranes were incubated in appropriate dilutions of the secondary HRP-linked antibody (goat-anti-rabbit IgG, goat-anti-mouse IgG, Santa Cruz, Dallas, TX, USA or donkey-anti-goat IgG, Novus Biologicals, Abingdon, United Kingdom) and detection was performed by using SuperSignal West Femto Maximum

Sensitivity Substrate (Thermo Scientific) or Amersham ECL Prime Western Blotting Detection Reagent (GE Healthcare Life Technologies) on an Intas ECL Chemocam Imager (Intas Science Imaging Instruments, Goettingen, Germany). Recorded images were analysed using LabImage 1D software (Kapelan Bio-Imaging, Leipzig, Germany).

Sample preparation and LC-MS/MS lipid mediator analysis ("Frankfurt panel")

Quantification of HETE and LTB4 was done in principle as described previously.[1] For analysis of 5-HETE, 12-HETE, 15-HETE and LTB_4, 150 - 200 µl supernatant were spiked with the corresponding deuterated internal standards and extracted by liquid-liquid-extraction using ethyl acetate. Analytes were separated using a Gemini NX C18 RP-LC-column (150 mm × 2 mm I.D., 5 µm particle size and 110 Å pore size from Phenomenex, Aschaffenburg, Germany) under gradient conditions with H_2O and acetonitrile as mobile phases, both containing 0.01% ammonia solution. The LC system was coupled to a mass spectrometer 5500 QTrap (Sciex, Darmstadt, Germany) equipped with a Turbo-V-source operating in negative electrospray ionization mode. Data Acquisition was done using Analyst Software V 1.6 and quantification was performed with MultiQuant Software V 3.0 (Sciex) employing the internal standard method (isotope dilution mass spectrometry).

For the analysis of prostanoids, 200 µl supernatant were spiked with isotopically labeled internal standards (PGE_2-d4, PGD_2-d4, TXB_2-d4, $PGF_2\alpha$-d4, 6-keto $PGF_1\alpha$-d4), 100 µl EDTA solution (0.15M) and 600 µl ethyl acetate. Samples were vortexed and centrifuged at 20,000 g for 5 min. The organic phase was removed, and the extraction was repeated with 600 µl ethyl acetate. The organic fractions were evaporated at a temperature of 45°C under a gentle stream of nitrogen. The residues were reconstituted with 50 µl of acetonitrile/H_2O/formic acid (20:80:0.0025, v/v/v) and transferred to glass vials.

The LC-MS/MS analysis was carried out using an Agilent 1290 Infinity LC system (Agilent, Waldbronn, Germany) coupled to a hybrid triple quadrupole linear ion trap mass spectrometer QTRAP 6500+ (Sciex) equipped with a Turbo-V-source operating in negative ESI mode. The chromatographic separation was conducted using a Synergi Hydro-RP column (150 × 2 mm, 4 µm particle size and 80 Å pore size; Phenomenex). A gradient program was employed at a flow rate of 300 µl/min. Mobile phase A was H_2O/formic acid (100:0.0025, v/v) and mobile phase B was acetonitrile/formic acid (100:0.0025, v/v). The analytes were separated under gradient conditions within 16 min. The injection volume was 10 µl. The gradient program started with 90% A for 1 min, then mobile phase A was decreased to 60% within 1 min, held for 1 min, further decreased to 50% within 1 min and held for 2 min. Within 2 min, mobile phase A was further decreased to 10% and held for 1 min. Within 1 min, the initial conditions were restored and the column was re-equilibrated for 6 min. Mass spectrometric parameters were set as follows: Ionspray voltage -4500 V, source temperature 500 °C, curtain gas 40 psi, nebulizer gas 40 psi and Turbo heater gas 60 psi. Both quadrupoles were running at unit resolution.

For analysis and quantification, Analyst Software 1.6 and Multiquant Software 3.0 (both Sciex) were used, employing the internal standard method (isotope dilution mass spectrometry). Calibration curves were constructed using linear regression with $1/x^2$ weighting.

Supplemental figure and table legends

Fig S1. LC-MS/MS spectrum of the 52 metabolites as labeled in the figure at a concentration of 1 ng/ml (10 ng/ml for PUFAs)

Fig S2. Gene expression profile and effect of IL-4 in MDM differentiated in the absence of TGFβ1 A Gene expression profile of MDM differentiated in the presence of GM-CSF ± TGF-β1 (n=7) **B** Gene expression of *ALOX5* and *IL1B* normalized to *GAPDH* expression of MDM differentiated ± TGF-β1 **C** Gene expression normalized to *GAPDH* expression of MDM differentiated with GM-CSF for 6 days then stimulated with 10 ng/ml IL-4 for 24h (n=6). Data are presented as mean + SD. Statistical significance was determined using Wilcoxon test.

Fig S3. Time course of eicosanoid production by human aMDM during stimulation with IL-4 or HDM+IL-4

A – C Time course of prostanoids (A), 5-HETE, 5-oxoETE and 15-HETE (B), leukotrienes (C) in supernatants of aMDM stimulated or not with 10 ng/ml IL-4 +/- 10 µg/ml HDM for 24h, 48h, 72h or 96h (n=7)

Fig S4. Mediator reprogramming by HDM does not depend on LPS or TLR2/4 signaling.

A-B COX and 5-LOX products (A), IL-6 and TNFα (B) formed by aMDM ± HDM ± antiTLR4 (10 µg/ml)/TLR2 (10 µg/ml) or polymyxin B (5 µg/ml) (n=5). Data shown as mean + SD. Statistical significance was determined using Friedmann test with Dunn's post test.

Fig S5. p38 MAPK mediates eicosanoid reprogramming, cytokine induction and the chemotaxic potential of human aMDM. A-B COX and 5-LOX products (A), IL-6 and TNFα (B) from aMDM ± 10 µg/ml HDM ± 1 µmol/l DBM-1285 (n=6), **C** Percentage of granulocytes migrating towards pooled supernatants (SN) of aMDM ± 10 µg/ml HDM ± 1 µmol/l DBM (n=5). Data are presented as mean + SD. Statistical significance was determined using Friedmann test with Dunn's post test (A) or Wilcoxon test (B).

Table S1. Analyte stock solutions with MRM parameters; DP: declustering potential, CE: collision energy and CXP: collision cell exit potential

Table S2. Internal standard stock solutions with MRM parameters; DP: declustering potential, CE: collision energy and CXP: collision cell exit potential

Table S3. Forward and reverse primers for qPCR

Table S4. Intraday accuracy and precision (RSD) of the LC-MS/MS panel at different concentration levels (0.1, 1 and 10 ng/ml, 10x higher for PUFAs, n = 3)

Table S5. Recovery and matrix effect at a concentration of 1 ng/ml

Table S6. Accuracy und precision/RSD after 48h at 4°C at a concentration of 0.1, 1 and 10 ng/ml; PUFAs are 10x higher concentrated

Table S7: Inter-3-day variability of accuracy and precision/RSD at 0.1, 1 and 10 ng/ml; PUFAs are 10x higher concentrated

Table S8. Limit of detection (LOD) and lower limit of quantitation (LLOQ) with correlation coefficient

Table S9. Comparison of Frankfurt and Munich LC-MS/MS panel; shown is mean ± SD of 6 different blood donors

Table S1: Analyte stock with MRM parameters: DP: declustering potential, CE: collision energy and CXP: collision cell exit potential

Metabolite	Stock Concentration (ng/µl)	Q1 (m/z)	Q3 (m/z)	RT (min)	DP (V)	CE (V)	CXP (V)
±11-HDHA	1	343.418	149.1	9.4	-20	-18	-13
±11,12-DHET	1	337.14	167.1	6.7	-60	-24	-17
±12,13-DiHOME	1	313.083	183	6	-70	-30	-9
±13-HDHA	1	343.273	192.9	8.9	-10	-18	-9
±17-HDHA	1	343.258	244.9	8.6	-100	-16	-11
±18-HEPE	1	317.208	259.2	6.9	-65	-14	-7
±4-HDHA	1	343.27	101	11	-25	-18	-7
±5,6-DHET	1	337.149	144.9	7.6	-80	-24	-13
±8(9)-DHET	1	337.328	126.9	7	-80	-26	-23
±9-HETE	1	319.19	167.2	9.7	-10	-20	-15
±9,10-DiHOME	1	313.186	201.1	6.2	-85	-28	-11
11(12)-EET	1	319.19	167	11.4	-65	-20	-27
11(S)-HETE	1	319.091	166.7	9.1	-95	-20	-11
12-oxo-ETE	1	317.112	153.2	9.2	-90	-20	-19
12(S)-HEPE	1	317.113	178.8	7.6	-35	-18	-25
12(S)-HETE	1	319.3	178.7	9.4	-70	-18	-7
13(S)-HODE	1	295.065	195.1	8.2	-15	-24	-21
14(15)-EET	1	319.152	218.8	10.4	-60	-16	-29
14(15)-EpETE	1	317.139	207	8.6	-50	-18	-21
15-oxo-ETE	1	317.124	113.2	8.5	-120	-22	-13
15(S)-HEPE	1	317.235	218.9	7.2	-75	-16	-17
15(S)-HETE	1	319.152	218.9	8.6	-35	-18	-39
15(S)-HETrE	1	321.322	221.2	9.9	-15	-20	-11
15(S)-HpETE	1	335.079	112.9	10	-55	-18	-9
20-HETE	1	319.09	245	7.4	-145	-20	-11
5-oxoETE	1	317.025	203	10.8	-65	-22	-35
5(6)-EET	1	319.045	191.2	11.7	-25	-14	-1
5(S)-HEPE	1	317.266	115.1	8	-95	-18	-15
5(S)-HETE	1	319.101	114.9	10.3	-15	-18	-7
5(S)-HpETE	1	335.064	166.9	9.6	-5	-22	-15
6-keto-$PGF_1\alpha$	1	369.09	162.9	1.4	-65	-36	-19
8-iso-$PGF_2\alpha$	1	353.16	193	2.5	-125	-38	-19
8(9)-EET	1	319.152	155	11.6	-130	-16	-15
9(S)-HODE	1	295.091	171.2	8.4	-110	-22	-23
LTB_4	1	335.12	195	5.6	-90	-20	-25
LTC_4	1	624.207	272.1	5.3	-100	-30	-11
LTD_4	1	495.204	177	5.5	-65	-26	-21
LTE_4	1	438.207	333	5.4	-70	-24	-39
LXA4	1	351.123	114.9	4.5	-50	-20	-7
MAR1	1	359.14	177.2	5.5	-120	-20	-23
PDX	1	359.14	153.1	5.5	-95	-20	-15
PGD_2	1	351.122	271.1	4.1	-60	-22	-11
PGE_2	1	351.057	271.3	3.8	-20	-26	-9
$PGF_2\alpha$	1	353.143	193.1	3.4	-130	-34	-21
RvD1	1	375.143	141	4.5	-75	-20	-13
RvE1	1	349.087	161	1.6	-90	-26	-19
TXB_2	1	369.082	169.1	2.5	-45	-24	-21
AA	10	303.153	258.9	12.7	-95	-26	-13
ALA	10	277.155	233.2	12.4	-140	-18	-11

DGLA	10	305.156	261.2	12.8	-110	-22	-9
DHA	10	327.122	283.2	12.6	-110	-14	-11
EPA	10	300.992	257	12.4	-5	-16	-25

Table S2: Internal standard stock with MRM parameters; DP: declustering potential, CE: collision energy and CXP: collision cell exit potential

Metabolite	Stock Concentration (ng/µl)	Q1 (m/z)	Q3 (m/z)	RT (min)	DP (V)	CE (V)	CXP (V)
11,12-DHET-d11	1	348.22	167.1	6.6	-80	-26	-9
8,9-DHET-d11	1	348.143	127	7	-85	-28	-13
11(12)-EET-d11	1	330.226	167	11.3	-70	-18	-13
12(S)-HETE-d8	1	327.119	184.5	9.2	-90	-20	-9
13(S)-HODE-d4	1	299.174	198.1	8.1	-95	-24	-11
15(S)-HETE-d8	1	327.122	226.1	8.4	-30	-18	-9
5-oxoETE-d7	1	324.177	210.2	10.8	-85	-24	-13
5(S)-HETE-d8	1	327.167	116	10.1	-15	-18	-7
6-keto-$PGF_1\alpha$-d4	1	373.079	167	1.4	-70	-36	-7
LTB_4-d4	1	339.12	197	5.6	-90	-20	-25
PGD_2-d4	1	355.105	275.3	4.1	-70	-22	-5
PGE_2-d4	1	355.173	275.2	3.8	-75	-24	-11
$PGF_2\alpha$-d4	1	357.212	313.3	3.4	-65	-24	-35
RvD1-d5	1	380.196	141	4.5	-155	-20	-17
TXB_2-d4	1	373.201	173	2.5	-60	-22	-21
AA-d8	10	311.09	267	12.6	-95	-26	-13
EPA-d5	10	306.246	262.2	12.4	-30	-16	-9

Table S3: Forward and reverse primers for qPCR

Gene	Forward Primer (5' - 3')	Reverse Primer (5' - 3')
PTGS2	GCTGGAACATGGAATTACCCA	CTTTCTGTACTGCGGGTGGAA
PTGES	TCAAGATGTACGTGGTGGCC	GAAAGGAGTAGACGAAGCCCAG
ALOX5	GATTGTCCCCATTGCCATCC	AGAAGGTGGGTGATGGTCTG
ALOX15	GGACACTTGATGGCTGAGGT	GTATCGCAGGTGGGGAATTA
TGM2	AGGCCCGTTTTCCACTAAGA	AGCAAAATGAAGTGGCCCAG
GAPDH	GAAGGTGAAGGTCGGAGT	GAAGATGGTGATGGGATTTC

Concentration	0.1 ng/ml		1 ng/ml		10 ng/ml	
Metabolites	**Accuracy (%)**	**RSD (%)**	**Accuracy (%)**	**RSD (%)**	**Accuracy (%)**	**RSD (%)**
±11-HDHA	95.26	45.26	121.52	15.42	121.64	11.70
±11,12-DHET	114.55	27.47	109.46	14.02	91.52	14.20
±12,13-DiHOME	NA	NA	103.87	13.80	104.35	18.12
±13-HDHA	NA	NA	97.90	13.64	103.55	13.31
±17-HDHA	140.48	53.19	110.44	2.88	112.29	10.95
±18-HEPE	NA	NA	104.93	11.59	101.24	13.04
±4-HDHA	155.63	24.76	117.30	19.22	105.17	13.64
±5,6-DHET	88.30	39.87	106.59	7.23	95.46	12.44
±8(9)-DHET	NA	NA	95.82	14.73	97.25	13.44
±9-HETE	96.67	37.91	126.38	14.66	121.23	12.55
±9,10-DiHOME	85.87	48.05	88.60	14.29	79.86	19.75
11(12)-EET	47.85	80.53	106.23	12.94	96.02	11.55
11(S)-HETE	119.79	23.47	100.35	16.36	88.94	14.76
12-oxo-ETE	276.86	5.94	59.81	26.45	26.17	79.04
12(S)-HEPE	59.16	98.57	101.71	14.13	96.00	13.21
12(S)-HETE	89.67	59.94	109.23	17.98	107.72	19.02
13(S)-HODE	60.27	99.28	104.32	15.45	98.05	13.79
14(15)-EET	NA	NA	82.28	19.54	96.21	11.39
14(15)-EpETE	NA	NA	53.59	47.43	99.43	9.59
15-oxo-ETE	52.15	41.83	101.50	9.74	96.07	14.01
15(S)-HEPE	18.35	114.94	101.20	13.46	100.33	11.79
15(S)-HETE	177.23	11.66	98.63	14.42	96.39	11.67
15(S)-HETrE	NA	NA	93.77	20.74	93.86	16.04
15(S)-HpETE	NA	NA	NA	NA	26.82	78.79
20-HETE	NA	NA	156.46	15.19	119.87	27.95
5-oxoETE	144.23	31.83	107.97	9.11	91.01	10.92
5(6)-EET	33.03	74.44	108.11	87.12	61.18	101.98
5(S)-HEPE	66.64	61.40	122.21	6.17	112.28	14.19
5(S)-HETE	83.48	83.86	102.42	18.91	91.63	13.80
5(S)-HpETE	NA	NA	NA	NA	NA	NA
6-keto-PGF_{1alpha}	124.16	3.38	143.04	7.08	119.90	10.69
8-iso-PGF_{2alpha}	51.63	21.08	109.82	21.53	110.56	13.18
8(9)-EET	79.63	10.88	102.80	12.53	100.64	10.85
9(S)-HODE	85.22	59.03	106.24	15.77	92.55	14.48
LTB_4	106.03	22.11	98.02	10.87	86.87	14.46
LTC_4	368.38	6.49	128.66	15.88	96.54	5.73
LTD_4	29.24	99.62	105.70	12.55	97.71	7.24
LTE_4	50.86	97.21	110.17	13.90	95.36	9.43
LXA4	42.19	73.46	82.47	13.64	79.78	23.44
MAR1	NA	NA	205.38	15.28	138.94	27.30
PDX	NA	NA	100.06	16.37	111.18	11.09
PGD_2	NA	NA	106.52	18.57	104.22	5.07
PGE_2	34.18	74.36	67.28	12.89	58.92	11.58
PGF_{2alpha}	NA	NA	99.12	12.34	97.98	13.33
RvD1	59.84	46.36	98.35	13.55	91.53	15.97
RvE1	179.13	12.56	117.52	18.10	119.98	7.01
TXB_2	125.72	26.63	112.53	2.47	97.03	4.52
AA	NA	NA	1108.92	39.52	142.08	47.69
ALA	NA	NA	82.53	NA	97.06	27.37
DGLA	NA	NA	400.56	19.18	117.29	24.34
DHA	NA	NA	2938.46	44.93	188.60	73.28

EPA	NA	NA	59.36	NA	82.43	28.66

Table S4: Accuracy and precision (RSD) at different concentration levels; 0.1, 1 and 10 ng/ml, n=4 individual extractions

Table S5: Recovery and matrix effect at 1 ng/ml (n=3 separate extractions)

Metabolite	Recovery ± SD	Matrix Effect ± SD
±11-HDHA	148.75 ± 34.92	108.16 ± 25.39
±11,12-DHET	118.03 ± 24.79	96.27 ± 20.22
±12,13-DiHOME	158.56 ± 51.27	112.19 ± 36.28
±13-HDHA	111.10 ± 22.94	94.03 ± 19.42
±17-HDHA	138.36 ± 24.21	108.51 ± 18.99
±18-HEPE	128.26 ± 26.47	93.40 ± 19.28
±4-HDHA	251.65 ± 54.23	210.88 ± 45.45
±5,6-DHET	144.45 ± 34.95	96.86 ± 23.44
±8(9)-DHET	126.83 ± 29.79	101.01 ± 23.73
±9-HETE	166.06 ± 25.38	112.10 ± 17.13
±9,10-DiHOME	130.83 ± 46.62	87.33 ± 31.11
11(12)-EET	116.46 ± 22.45	92.55 ± 17.84
11(S)-HETE	122.57 ± 25.84	105.81 ± 22.31
12-oxo-ETE	6.76 ± 2.71	27.40 ± 15.01
12(S)-HEPE	146.17 ± 38.96	113.53 ± 30.26
12(S)-HETE	181.59 ± 34.31	131.64 ± 24.87
13(S)-HODE	105.21 ± 23.16	103.45 ± 22.77
14(15)-EET	162.87 ± 32.5	102.76 ± 20.5
14(15)-EpETE	109.40 ± 22.31	86.10 ± 17.56
15-oxo-ETE	121.15 ± 27.23	98.26 ± 22.08
15(S)-HEPE	136.25 ± 33.54	106.32 ± 26.17
15(S)-HETE	123.92 ± 22.27	88.43 ± 15.89
15(S)-HETrE	134.78 ± 31.85	105.85 ± 25.01
15(S)-HpETE	NA	NA
20-HETE	141.68 ± 35.5	96.21 ± 24.11
5-oxoETE	68.73 ± 18.59	89.37 ± 24.17
5(6)-EET	25.03 ± 7.83	170.46 ± 53.33
5(S)-HEPE	114.64 ± 24.15	105.71 ± 22.27
5(S)-HETE	190.21 ± 40.9	116.98 ± 25.15
5(S)-HpETE	33.69 ± 9.45	97.79 ± 27.43
6-keto-$PGF_1\alpha$	136.13 ± 26.51	92.98 ± 18.11
8-iso-$PGF_2\alpha$	312.89 ± 66.64	160.30 ± 34.14
8(9)-EET	118.49 ± 27.25	92.00 ± 21.16
9(S)-HODE	132.93 ± 29.76	102.12 ± 22.86
LTB_4	120.93 ± 31.32	91.29 ± 23.64
LTC_4	81.91 ± 24.9	75.42 ± 22.92
LTD_4	88.45 ± 25.56	76.89 ± 22.22
LTE_4	82.85 ± 23.48	79.60 ± 22.56
LXA4	131.71 ± 27.76	99.16 ± 20.9
MAR1	138.35 ± 36.68	103.82 ± 27.52
PDX	133.66 ± 37.96	96.30 ± 27.35
PGD_2	68.76 ± 22.87	82.16 ± 27.33
PGE_2	123.64 ± 20.24	92.57 ± 15.16
$PGF_2\alpha$	127.10 ± 30.71	98.41 ± 23.78
RvD1	116.18 ± 23.24	89.59 ± 17.92
RvE1	170.89 ± 28.26	99.91 ± 16.52
TXB_2	118.69 ± 22.51	96.24 ± 18.52
AA	785.36 ± 166.65	447.00 ± 94.85
ALA	146.64 ± 32.26	114.75 ± 25.24
DGLA	316.64 ± 47.09	208.02 ± 30.94
DHA	410.34 ± 95.54	219.43 ± 51.09
EPA	335.53 ± 73.83	241.74 ± 53.19

Table S6: Accuracy und precision/RSD after 48 h at 4 °C at a concentration of 0.1, 1 and 10 ng/ml; PUFAs are 10x higher concentrated (n =3)

Metabolites	Accuracy (%)	RSD (%)	Accuracy (%)	RSD (%)	Accuracy (%)	RSD (%)
concentration	0.1 ng/ml		1 ng/ml		10 ng/ml	
±11-HDHA	/	/	81.97	1.71	106.30	3.31
±11,12-DHET	14.45	121.38	93.16	1.18	114.49	2.17
±12,13-DiHOME	95.82	4.85	81.85	0.69	104.79	2.06
±13-HDHA	69.08	12.16	80.67	1.94	107.75	4.82
±17-HDHA	/	/	81.25	9.46	104.86	4.49
±18-HEPE	/	/	77.80	5.35	106.41	3.22
±4-HDHA	9.34	79.80	74.67	5.42	105.21	4.80
±5,6-DHET	91.07	6.48	94.39	0.37	126.88	2.58
±8(9)-DHET	93.83	10.55	81.04	1.61	110.97	3.48
±9-HETE	98.17	4.01	89.75	0.45	108.58	4.59
±9,10-DiHOME	93.61	7.10	86.21	2.69	110.46	2.16
11(12)-EET	16.38	/	78.01	5.31	104.23	2.20
11(S)-HETE	/	/	86.91	2.52	107.20	4.12
12-oxo-ETE	8.88	7.86	38.33	7.90	58.59	3.53
12(S)-HEPE	100.63	6.19	79.00	5.40	108.31	1.31
12(S)-HETE	89.63	2.50	54.16	6.54	104.59	4.06
13(S)-HODE	87.70	4.16	86.02	1.72	107.66	2.87
14(15)-EET	4.95	/	87.83	0.69	108.09	7.81
14(15)-EpETE	41.15	46.16	89.36	4.65	106.74	5.28
15-oxo-ETE	101.07	9.48	88.80	1.54	103.02	7.01
15(S)-HEPE	/	/	86.10	1.55	107.15	0.21
15(S)-HETE	489.52	5.98	217.44	2.00	103.00	2.73
15(S)-HETrE	92.07	5.57	89.35	2.85	107.80	2.60
15(S)-HpETE	46.20	3.10	78.55	6.44	114.89	7.94
20-HETE	25.37	4.26	311.67	0.57	177.37	3.15
5-oxoETE	31.30	25.67	79.96	5.41	110.53	2.44
5(6)-EET	259.67	/	155.06	59.20	98.35	104.00
5(S)-HEPE	100.56	8.21	85.99	6.41	108.03	3.69
5(S)-HETE	/	/	98.21	3.80	106.58	2.23
5(S)-HpETE	37.53	36.77	/	/	117.13	5.31
6-keto-$PGF_1\alpha$	185.28	22.91	333.08	3.21	184.08	0.92
8-iso-$PGF_2\alpha$	86.35	7.62	97.69	2.65	113.37	4.97
8(9)-EET	3.01	/	83.15	9.74	109.94	1.15
9(S)-HODE	92.17	8.14	96.40	0.98	109.02	2.79
LTB_4	36.48	11.50	87.25	1.85	106.77	1.32
LTC_4	87.73	6.46	60.09	14.77	95.68	5.38
LTD_4	102.99	1.30	80.80	0.59	107.33	2.76
LTE_4	91.40	2.57	90.12	3.42	119.59	4.24
LXA4	14.83	/	84.79	4.75	103.93	2.41
MAR1	396.85	1.41	398.73	3.21	211.92	4.23
PDX	90.21	4.62	92.74	1.53	115.08	1.53
PGD_2	85.04	4.41	97.10	0.98	109.62	2.13
PGE_2	94.22	8.66	92.20	0.74	109.63	2.74
$PGF_2\alpha$	86.21	4.13	92.01	0.80	112.21	2.68
RvD1	86.59	3.25	84.60	1.72	104.69	2.99
RvE1	382.67	16.31	370.75	7.25	191.90	1.41
TXB_2	98.71	4.77	83.93	1.18	101.07	3.57
AA	96.85	15.07	98.72	2.11	111.05	2.66
ALA	76.26	7.09	121.03	3.22	128.08	2.53

DGLA	19.67	/	91.67	4.99	104.61	2.28
DHA	107.96	0.37	69.02	4.96	57.28	5.67
EPA	125.55	2.74	125.82	0.96	134.70	2.11

Table S7: Inter-3-day variability of accuracy and precision/RSD at 0.1, 1 and 10 ng/ml; PUFAs are 10x higher concentrated (n=3)

Metabolites	Accuracy (%)	RSD (%)	Accuracy (%)	RSD (%)	Accuracy (%)	RSD (%)
concentration	0.1 ng/ml		1 ng/ml		10 ng/ml	
±11-HDHA	143.02	30.76	103.49	8.79	103.82	4.95
±11,12-DHET	119.68	1.93	102.83	6.10	100.59	2.20
±12,13-DiHOME	140.53	14.74	102.67	4.62	100.21	1.90
±13-HDHA	180.04	28.11	117.19	13.53	97.64	6.61
±17-HDHA	136.92	15.69	106.39	3.10	101.04	4.52
±18-HEPE	148.14	10.58	110.29	0.99	103.43	5.22
±4-HDHA	202.72	23.32	109.19	23.01	120.00	17.31
±5,6-DHET	141.55	19.66	106.84	4.04	100.89	3.81
±8(9)-DHET	130.38	20.59	106.18	8.78	101.41	5.02
±9-HETE	107.88	10.70	84.90	14.84	87.49	20.97
±9,10-DiHOME	172.42	16.37	116.61	10.92	101.21	7.68
11(12)-EET	142.84	16.30	113.63	2.28	104.05	6.25
11(S)-HETE	144.99	28.43	107.75	6.61	101.55	1.78
12-oxo-ETE	NA	NA	100.58	47.04	90.25	45.12
12(S)-HEPE	166.38	24.39	113.60	3.10	98.01	5.25
12(S)-HETE	230.28	60.98	101.39	1.03	101.57	3.36
13(S)-HODE	166.54	7.11	103.40	6.18	102.73	2.53
14(15)-EET	94.60	15.53	112.79	13.23	101.73	6.35
14(15)-EpETE	140.26	28.50	103.28	9.92	104.94	5.53
15-oxo-ETE	152.39	13.43	113.81	2.28	108.03	6.57
15(S)-HEPE	130.70	9.05	102.36	8.71	101.82	3.17
15(S)-HETE	138.53	16.73	107.79	4.94	111.99	8.42
15(S)-HETrE	138.79	27.16	112.88	8.87	106.01	9.23
15(S)-HpETE	NA	NA	125.99	NA	62.15	86.12
20-HETE	105.16	21.19	104.98	7.27	104.69	1.98
5-oxoETE	128.17	10.70	103.40	10.31	114.85	24.63
5(6)-EET	139.76	23.86	105.50	12.07	91.75	14.08
5(S)-HEPE	149.54	7.15	106.10	2.94	110.07	10.56
5(S)-HETE	231.21	44.70	113.16	7.13	101.12	4.38
5(S)-HpETE	NA	NA	NA	NA	NA	NA
6-keto-$PGF_1\alpha$	102.01	12.82	91.50	6.49	96.75	9.37
8-iso-$PGF_2\alpha$	113.92	9.52	103.22	7.63	103.40	15.29
8(9)-EET	150.18	16.08	111.40	2.65	112.48	9.48
9(S)-HODE	172.33	24.73	105.72	6.30	102.03	4.08
LTB_4	130.61	22.99	107.42	7.22	100.07	2.30
LTC_4	119.86	32.20	101.37	8.37	101.13	3.95
LTD_4	140.30	31.13	107.71	6.63	100.06	3.07
LTE_4	120.35	24.06	109.84	3.07	103.58	5.93
LXA4	134.56	7.52	111.38	5.75	108.98	8.84
MAR1	135.97	21.48	104.56	8.88	102.06	3.55
PDX	130.64	18.81	105.48	13.01	101.45	1.54
PGD_2	131.20	21.28	103.53	7.04	100.79	3.62
PGE_2	125.20	22.41	109.18	5.68	103.26	3.79
$PGF_2\alpha$	147.94	21.55	115.13	4.68	105.34	4.77
RvD1	126.87	20.61	104.69	3.22	101.95	2.58
RvE1	98.36	3.04	98.72	5.59	95.94	14.67
TXB_2	125.13	20.40	104.07	2.74	106.39	7.99
AA	349.17	26.16	120.76	40.71	125.30	25.53
ALA	216.22	55.50	109.50	12.29	96.96	0.97

DGLA	2846.77	134.75	91.21	63.96	68.53	68.78
DHA	10738.50	142.89	1448.42	114.05	118.85	4.64
EPA	296.48	56.65	120.56	44.51	85.10	16.89

Table S8: Limit of detection (LOD) and lower limit of quantitation (LLOQ) with correlation coefficient

Metabolite	LOD (ng/ml)	LLOQ (ng/ml)	Correlation Coefficient
±11-HDHA	0.05	0.5	0.99999
±11,12-DHET	0.005	0.05	0.99999
±12,13-DiHOME	0.005	0.5	0.99993
±13-HDHA	0.1	1	0.99978
±17-HDHA	0.005	1	0.99999
±18-HEPE	0.05	0.5	0.99993
±4-HDHA	0.5	1	1
±5,6-DHET	0.05	0.05	1
±8(9)-DHET	0.005	0.5	0.99992
±9-HETE	0.005	0.5	0.99999
±9,10-DiHOME	0.1	1	0.9999
11(12)-EET	0.005	0.5	0.99999
11(S)-HETE	0.005	0.05	0.99993
12-oxo-ETE	0.5	0.5	0.99977
12(S)-HEPE	0.5	1	0.99998
12(S)-HETE	0.005	1	0.99999
13(S)-HODE	0.1	0.5	0.99999
14(15)-EET	0.01	0.5	0.99989
14(15)-EpETE	0.1	0.5	0.99885
15-oxo-ETE	0.05	0.5	0.99995
15(S)-HEPE	0.05	0.5	0.99992
15(S)-HETE	0.25	0.05	0.99994
15(S)-HETrE	0.1	10	0.99984
15(S)-HpETE	0.005	NA	0.99958
20-HETE	0.01	1	0.99946
5-oxoETE	0.005	0.05	0.99992
5(6)-EET	0.01	NA	0.99955
5(S)-HEPE	0.05	0.05	0.99999
5(S)-HETE	0.5	0.05	1
5(S)-HpETE	NA	NA	N/A
6-keto-$PGF_1\alpha$	0.01	0.1	0.99958
8-iso-$PGF_2\alpha$	0.005	0.5	0.99951
8(9)-EET	0.05	0.1	0.99994
9(S)-HODE	0.1	0.05	0.99998
LTB_4	0.005	0.05	0.99998
LTC_4	0.005	0.005	0.99959
LTD_4	0.005	0.5	0.99988
LTE_4	0.005	0.5	0.99998
LXA4	0.005	0.5	0.99996
MAR1	0.005	1	0.99988
PDX	0.005	0.5	0.99945
PGD_2	0.005	0.5	0.99975
PGE_2	0.005	0.5	0.99947
$PGF_2\alpha$	0.005	0.5	0.99995
RvD1	0.005	0.5	0.99999
RvE1	0.05	0.05	0.99999
TXB_2	0.005	0.25	0.99996
AA	500	100	0.99948
ALA	50	100	0.9995
DGLA	50	1	0.99986
DHA	500	NA	0.99568
EPA	50	100	0.99911

Table S9: Comparison of Frankfurt and Munich LC-MS/MS panels, data are shown as mean ± SD for 6 different blood donors.

Metabolite	Frankfurt (ng/ml) (method 2)	Munich (ng/ml) (method 1)
PGD_2	0.009 ± 0.005	0.012 ± 0.008
PGE_2	0.012 ± 0.012	0.008 ± 0.007
$PGF_2\alpha$	0.018 ± 0.017	0.050 ± 0.065
LTB_4	9.061 ± 4.342	29.097 ± 34.562
TXB_2	0.298 ± 0.380	0.186 ± 0.210
5-HETE	8.411 ± 9.181	11.913 ± 12.668
15-HETE	0.237 ± 0.547	0.110 ± 0.066

~~Table S10: Levels of eicosanoids detected in BALF or intestinal culture supernatant of naïve mice or mice infected with *Nippostrongylus brasiliensis* (*Nb*) or Heligmosomoides polygyrus bakeri (*Hpb*)~~; ~~concentrations in pg/ml ± SD, n=5 for naïve mice and n=3-4 for infected mice~~

~~Metabolite~~	~~BALF, naïve~~	~~BALF, helminth (*Nb*)~~	~~intestine, naïve~~	~~intestine, helminth (*Hpb*)~~
~~PGE_2~~	~~<LOD~~	~~122.0 ± 68.0~~	~~16.9 ± 7.0~~	~~16600 ± 4862~~
~~PGD_2~~	~~<LOD~~	~~64.5 ± 1.0~~	~~25.6 ± 11.6~~	~~511.9 ± 149.3~~
~~TXB_2~~	~~<LOD~~	~~66.9 ± 17.2~~	~~9.1 ± 3.7~~	~~4180 ± 518.6~~
~~$PGF_{2\alpha}$~~	~~<LOD~~	~~62.5 ± 4.4~~	~~0.2 ± 0.2~~	~~28490 ± 8135~~
~~LTB_4~~	~~46.0 ± 64.1~~	~~100.8 ± 49.5~~	~~<LOD~~	~~<LOD~~
~~5-HETE~~	~~12.0 ± 24.0~~	~~<LOD~~	~~0.3 ± 0.4~~	~~<LOD~~
~~12-HETE~~	~~233.0 ± 63.7~~	~~1995 ± 2355~~	~~17.3 ± 12.1~~	~~60070 ± 23620~~
~~15-HETE~~	~~26.8 ± 31.7~~	~~141.2 ± 161.8~~	~~2.3 ± 1.6~~	~~73120 ± 16380~~

Table S1: Analyte stock with MRM parameters: DP: declustering potential, CE: collision energy and CXP: collision cell exit potential

Metabolite	Stock Concentration (ng/µl)	Q1 (m/z)	Q3 (m/z)	RT (min)	DP (V)	CE (V)	CXP (V)
±11-HDHA	1	343.418	149.1	9.4	-20	-18	-13
±11,12-DHET	1	337.14	167.1	6.7	-60	-24	-17
±12,13-DiHOME	1	313.083	183	6	-70	-30	-9
±13-HDHA	1	343.273	192.9	8.9	-10	-18	-9
±17-HDHA	1	343.258	244.9	8.6	-100	-16	-11
±18-HEPE	1	317.208	259.2	6.9	-65	-14	-7
±4-HDHA	1	343.27	101	11	-25	-18	-7
±5,6-DHET	1	337.149	144.9	7.6	-80	-24	-13
±8(9)-DHET	1	337.328	126.9	7	-80	-26	-23
±9-HETE	1	319.19	167.2	9.7	-10	-20	-15
±9,10-DiHOME	1	313.186	201.1	6.2	-85	-28	-11
11(12)-EET	1	319.19	167	11.4	-65	-20	-27
11(S)-HETE	1	319.091	166.7	9.1	-95	-20	-11
12-oxo-ETE	1	317.112	153.2	9.2	-90	-20	-19
12(S)-HEPE	1	317.113	178.8	7.6	-35	-18	-25
12(S)-HETE	1	319.3	178.7	9.4	-70	-18	-7
13(S)-HODE	1	295.065	195.1	8.2	-15	-24	-21
14(15)-EET	1	319.152	218.8	10.4	-60	-16	-29
14(15)-EpETE	1	317.139	207	8.6	-50	-18	-21
15-oxo-ETE	1	317.124	113.2	8.5	-120	-22	-13
15(S)-HEPE	1	317.235	218.9	7.2	-75	-16	-17
15(S)-HETE	1	319.152	218.9	8.6	-35	-18	-39
15(S)-HETrE	1	321.322	221.2	9.9	-15	-20	-11
15(S)-HpETE	1	335.079	112.9	10	-55	-18	-9
20-HETE	1	319.09	245	7.4	-145	-20	-11
5-oxoETE	1	317.025	203	10.8	-65	-22	-35
5(6)-EET	1	319.045	191.2	11.7	-25	-14	-1
5(S)-HEPE	1	317.266	115.1	8	-95	-18	-15
5(S)-HETE	1	319.101	114.9	10.3	-15	-18	-7
5(S)-HpETE	1	335.064	166.9	9.6	-5	-22	-15
6-keto-$PGF_1\alpha$	1	369.09	162.9	1.4	-65	-36	-19
8-iso-$PGF_2\alpha$	1	353.16	193	2.5	-125	-38	-19
8(9)-EET	1	319.152	155	11.6	-130	-16	-15
9(S)-HODE	1	295.091	171.2	8.4	-110	-22	-23
LTB_4	1	335.12	195	5.6	-90	-20	-25
LTC_4	1	624.207	272.1	5.3	-100	-30	-11
LTD_4	1	495.204	177	5.5	-65	-26	-21
LTE_4	1	438.207	333	5.4	-70	-24	-39
LXA4	1	351.123	114.9	4.5	-50	-20	-7
MAR1	1	359.14	177.2	5.5	-120	-20	-23
PDX	1	359.14	153.1	5.5	-95	-20	-15
PGD_2	1	351.122	271.1	4.1	-60	-22	-11
PGE_2	1	351.057	271.3	3.8	-20	-26	-9
$PGF_2\alpha$	1	353.143	193.1	3.4	-130	-34	-21
RvD1	1	375.143	141	4.5	-75	-20	-13
RvE1	1	349.087	161	1.6	-90	-26	-19
TXB_2	1	369.082	169.1	2.5	-45	-24	-21
AA	10	303.153	258.9	12.7	-95	-26	-13
ALA	10	277.155	233.2	12.4	-140	-18	-11

DGLA	10	305.156	261.2	12.8	-110	-22	-9
DHA	10	327.122	283.2	12.6	-110	-14	-11
EPA	10	300.992	257	12.4	-5	-16	-25

Table S2: Internal standard stock with MRM parameters; DP: declustering potential, CE: collision energy and CXP: collision cell exit potential

Metabolite	Stock Concentration (ng/µl)	Q1 (m/z)	Q3 (m/z)	RT (min)	DP (V)	CE (V)	CXP (V)
11,12-DHET-d11	1	348.22	167.1	6.6	-80	-26	-9
8,9-DHET-d11	1	348.143	127	7	-85	-28	-13
11(12)-EET-d11	1	330.226	167	11.3	-70	-18	-13
12(S)-HETE-d8	1	327.119	184.5	9.2	-90	-20	-9
13(S)-HODE-d4	1	299.174	198.1	8.1	-95	-24	-11
15(S)-HETE-d8	1	327.122	226.1	8.4	-30	-18	-9
5-oxoETE-d7	1	324.177	210.2	10.8	-85	-24	-13
5(S)-HETE-d8	1	327.167	116	10.1	-15	-18	-7
6-keto-$PGF_1\alpha$-d4	1	373.079	167	1.4	-70	-36	-7
LTB_4-d4	1	339.12	197	5.6	-90	-20	-25
PGD_2-d4	1	355.105	275.3	4.1	-70	-22	-5
PGE_2-d4	1	355.173	275.2	3.8	-75	-24	-11
$PGF_2\alpha$-d4	1	357.212	313.3	3.4	-65	-24	-35
RvD1-d5	1	380.196	141	4.5	-155	-20	-17
TXB_2-d4	1	373.201	173	2.5	-60	-22	-21
AA-d8	10	311.09	267	12.6	-95	-26	-13
EPA-d5	10	306.246	262.2	12.4	-30	-16	-9

Table S3: Forward and reverse primers for qPCR

Gene	Forward Primer (5' - 3')	Reverse Primer (5' - 3')
PTGS2	GCTGGAACATGGAATTACCCA	CTTTCTGTACTGCGGGTGGAA
PTGES	TCAAGATGTACGTGGTGGCC	GAAAGGAGTAGACGAAGCCCAG
ALOX5	GATTGTCCCCATTGCCATCC	AGAAGGTGGGTGATGGTCTG
ALOX15	GGACACTTGATGGCTGAGGT	GTATCGCAGGTGGGGAATTA
TGM2	AGGCCCGTTTTCCACTAAGA	AGCAAAATGAAGTGGCCCAG
GAPDH	GAAGGTGAAGGTCGGAGT	GAAGATGGTGATGGGATTTC

Concentration	0.1 ng/ml		1 ng/ml		10 ng/ml	
Metabolites	**Accuracy (%)**	**RSD (%)**	**Accuracy (%)**	**RSD (%)**	**Accuracy (%)**	**RSD (%)**
±11-HDHA	95.26	45.26	121.52	15.42	121.64	11.70
±11,12-DHET	114.55	27.47	109.46	14.02	91.52	14.20
±12,13-DiHOME	NA	NA	103.87	13.80	104.35	18.12
±13-HDHA	NA	NA	97.90	13.64	103.55	13.31
±17-HDHA	140.48	53.19	110.44	2.88	112.29	10.95
±18-HEPE	NA	NA	104.93	11.59	101.24	13.04
±4-HDHA	155.63	24.76	117.30	19.22	105.17	13.64
±5,6-DHET	88.30	39.87	106.59	7.23	95.46	12.44
±8(9)-DHET	NA	NA	95.82	14.73	97.25	13.44
±9-HETE	96.67	37.91	126.38	14.66	121.23	12.55
±9,10-DiHOME	85.87	48.05	88.60	14.29	79.86	19.75
11(12)-EET	47.85	80.53	106.23	12.94	96.02	11.55
11(S)-HETE	119.79	23.47	100.35	16.36	88.94	14.76
12-oxo-ETE	276.86	5.94	59.81	26.45	26.17	79.04
12(S)-HEPE	59.16	98.57	101.71	14.13	96.00	13.21
12(S)-HETE	89.67	59.94	109.23	17.98	107.72	19.02
13(S)-HODE	60.27	99.28	104.32	15.45	98.05	13.79
14(15)-EET	NA	NA	82.28	19.54	96.21	11.39
14(15)-EpETE	NA	NA	53.59	47.43	99.43	9.59
15-oxo-ETE	52.15	41.83	101.50	9.74	96.07	14.01
15(S)-HEPE	18.35	114.94	101.20	13.46	100.33	11.79
15(S)-HETE	177.23	11.66	98.63	14.42	96.39	11.67
15(S)-HETrE	NA	NA	93.77	20.74	93.86	16.04
15(S)-HpETE	NA	NA	NA	NA	26.82	78.79
20-HETE	NA	NA	156.46	15.19	119.87	27.95
5-oxoETE	144.23	31.83	107.97	9.11	91.01	10.92
5(6)-EET	33.03	74.44	108.11	87.12	61.18	101.98
5(S)-HEPE	66.64	61.40	122.21	6.17	112.28	14.19
5(S)-HETE	83.48	83.86	102.42	18.91	91.63	13.80
5(S)-HpETE	NA	NA	NA	NA	NA	NA
6-keto-PGF_{1alpha}	124.16	3.38	143.04	7.08	119.90	10.69
8-iso-PGF_{2alpha}	51.63	21.08	109.82	21.53	110.56	13.18
8(9)-EET	79.63	10.88	102.80	12.53	100.64	10.85
9(S)-HODE	85.22	59.03	106.24	15.77	92.55	14.48
LTB_4	106.03	22.11	98.02	10.87	86.87	14.46
LTC_4	368.38	6.49	128.66	15.88	96.54	5.73
LTD_4	29.24	99.62	105.70	12.55	97.71	7.24
LTE_4	50.86	97.21	110.17	13.90	95.36	9.43
LXA4	42.19	73.46	82.47	13.64	79.78	23.44
MAR1	NA	NA	205.38	15.28	138.94	27.30
PDX	NA	NA	100.06	16.37	111.18	11.09
PGD_2	NA	NA	106.52	18.57	104.22	5.07
PGE_2	34.18	74.36	67.28	12.89	58.92	11.58
PGF_{2alpha}	NA	NA	99.12	12.34	97.98	13.33
RvD1	59.84	46.36	98.35	13.55	91.53	15.97
RvE1	179.13	12.56	117.52	18.10	119.98	7.01
TXB_2	125.72	26.63	112.53	2.47	97.03	4.52
AA	NA	NA	1108.92	39.52	142.08	47.69
ALA	NA	NA	82.53	NA	97.06	27.37
DGLA	NA	NA	400.56	19.18	117.29	24.34
DHA	NA	NA	2938.46	44.93	188.60	73.28

EPA	NA	NA	59.36	NA	82.43	28.66

Table S4: Accuracy and precision (RSD) at different concentration levels; 0.1, 1 and 10 ng/ml, n=4 individual extractions

Table S5: Recovery and matrix effect at 1 ng/ml (n=3 separate extractions)

Metabolite	Recovery ± SD	Matrix Effect ± SD
±11-HDHA	148.75 ± 34.92	108.16 ± 25.39
±11,12-DHET	118.03 ± 24.79	96.27 ± 20.22
±12,13-DiHOME	158.56 ± 51.27	112.19 ± 36.28
±13-HDHA	111.10 ± 22.94	94.03 ± 19.42
±17-HDHA	138.36 ± 24.21	108.51 ± 18.99
±18-HEPE	128.26 ± 26.47	93.40 ± 19.28
±4-HDHA	251.65 ± 54.23	210.88 ± 45.45
±5,6-DHET	144.45 ± 34.95	96.86 ± 23.44
±8(9)-DHET	126.83 ± 29.79	101.01 ± 23.73
±9-HETE	166.06 ± 25.38	112.10 ± 17.13
±9,10-DiHOME	130.83 ± 46.62	87.33 ± 31.11
11(12)-EET	116.46 ± 22.45	92.55 ± 17.84
11(S)-HETE	122.57 ± 25.84	105.81 ± 22.31
12-oxo-ETE	6.76 ± 2.71	27.40 ± 15.01
12(S)-HEPE	146.17 ± 38.96	113.53 ± 30.26
12(S)-HETE	181.59 ± 34.31	131.64 ± 24.87
13(S)-HODE	105.21 ± 23.16	103.45 ± 22.77
14(15)-EET	162.87 ± 32.5	102.76 ± 20.5
14(15)-EpETE	109.40 ± 22.31	86.10 ± 17.56
15-oxo-ETE	121.15 ± 27.23	98.26 ± 22.08
15(S)-HEPE	136.25 ± 33.54	106.32 ± 26.17
15(S)-HETE	123.92 ± 22.27	88.43 ± 15.89
15(S)-HETrE	134.78 ± 31.85	105.85 ± 25.01
15(S)-HpETE	NA	NA
20-HETE	141.68 ± 35.5	96.21 ± 24.11
5-oxoETE	68.73 ± 18.59	89.37 ± 24.17
5(6)-EET	25.03 ± 7.83	170.46 ± 53.33
5(S)-HEPE	114.64 ± 24.15	105.71 ± 22.27
5(S)-HETE	190.21 ± 40.9	116.98 ± 25.15
5(S)-HpETE	33.69 ± 9.45	97.79 ± 27.43
6-keto-$PGF_1\alpha$	136.13 ± 26.51	92.98 ± 18.11
8-iso-$PGF_2\alpha$	312.89 ± 66.64	160.30 ± 34.14
8(9)-EET	118.49 ± 27.25	92.00 ± 21.16
9(S)-HODE	132.93 ± 29.76	102.12 ± 22.86
LTB_4	120.93 ± 31.32	91.29 ± 23.64
LTC_4	81.91 ± 24.9	75.42 ± 22.92
LTD_4	88.45 ± 25.56	76.89 ± 22.22
LTE_4	82.85 ± 23.48	79.60 ± 22.56
LXA4	131.71 ± 27.76	99.16 ± 20.9
MAR1	138.35 ± 36.68	103.82 ± 27.52
PDX	133.66 ± 37.96	96.30 ± 27.35
PGD_2	68.76 ± 22.87	82.16 ± 27.33
PGE_2	123.64 ± 20.24	92.57 ± 15.16
$PGF_2\alpha$	127.10 ± 30.71	98.41 ± 23.78
RvD1	116.18 ± 23.24	89.59 ± 17.92
RvE1	170.89 ± 28.26	99.91 ± 16.52
TXB_2	118.69 ± 22.51	96.24 ± 18.52
AA	785.36 ± 166.65	447.00 ± 94.85
ALA	146.64 ± 32.26	114.75 ± 25.24
DGLA	316.64 ± 47.09	208.02 ± 30.94
DHA	410.34 ± 95.54	219.43 ± 51.09
EPA	335.53 ± 73.83	241.74 ± 53.19

Table S6: Accuracy und precision/RSD after 48 h at 4 °C at a concentration of 0.1, 1 and 10 ng/ml; PUFAs are 10x higher concentrated (n =3)

Metabolites	Accuracy (%)	RSD (%)	Accuracy (%)	RSD (%)	Accuracy (%)	RSD (%)
concentration	0.1 ng/ml		1 ng/ml		10 ng/ml	
±11-HDHA	/	/	81.97	1.71	106.30	3.31
±11,12-DHET	14.45	121.38	93.16	1.18	114.49	2.17
±12,13-DiHOME	95.82	4.85	81.85	0.69	104.79	2.06
±13-HDHA	69.08	12.16	80.67	1.94	107.75	4.82
±17-HDHA	/	/	81.25	9.46	104.86	4.49
±18-HEPE	/	/	77.80	5.35	106.41	3.22
±4-HDHA	9.34	79.80	74.67	5.42	105.21	4.80
±5,6-DHET	91.07	6.48	94.39	0.37	126.88	2.58
±8(9)-DHET	93.83	10.55	81.04	1.61	110.97	3.48
±9-HETE	98.17	4.01	89.75	0.45	108.58	4.59
±9,10-DiHOME	93.61	7.10	86.21	2.69	110.46	2.16
11(12)-EET	16.38	/	78.01	5.31	104.23	2.20
11(S)-HETE	/	/	86.91	2.52	107.20	4.12
12-oxo-ETE	8.88	7.86	38.33	7.90	58.59	3.53
12(S)-HEPE	100.63	6.19	79.00	5.40	108.31	1.31
12(S)-HETE	89.63	2.50	54.16	6.54	104.59	4.06
13(S)-HODE	87.70	4.16	86.02	1.72	107.66	2.87
14(15)-EET	4.95	/	87.83	0.69	108.09	7.81
14(15)-EpETE	41.15	46.16	89.36	4.65	106.74	5.28
15-oxo-ETE	101.07	9.48	88.80	1.54	103.02	7.01
15(S)-HEPE	/	/	86.10	1.55	107.15	0.21
15(S)-HETE	489.52	5.98	217.44	2.00	103.00	2.73
15(S)-HETrE	92.07	5.57	89.35	2.85	107.80	2.60
15(S)-HpETE	46.20	3.10	78.55	6.44	114.89	7.94
20-HETE	25.37	4.26	311.67	0.57	177.37	3.15
5-oxoETE	31.30	25.67	79.96	5.41	110.53	2.44
5(6)-EET	259.67	/	155.06	59.20	98.35	104.00
5(S)-HEPE	100.56	8.21	85.99	6.41	108.03	3.69
5(S)-HETE	/	/	98.21	3.80	106.58	2.23
5(S)-HpETE	37.53	36.77	/	/	117.13	5.31
6-keto-$PGF_1\alpha$	185.28	22.91	333.08	3.21	184.08	0.92
8-iso-$PGF_2\alpha$	86.35	7.62	97.69	2.65	113.37	4.97
8(9)-EET	3.01	/	83.15	9.74	109.94	1.15
9(S)-HODE	92.17	8.14	96.40	0.98	109.02	2.79
LTB_4	36.48	11.50	87.25	1.85	106.77	1.32
LTC_4	87.73	6.46	60.09	14.77	95.68	5.38
LTD_4	102.99	1.30	80.80	0.59	107.33	2.76
LTE_4	91.40	2.57	90.12	3.42	119.59	4.24
LXA4	14.83	/	84.79	4.75	103.93	2.41
MAR1	396.85	1.41	398.73	3.21	211.92	4.23
PDX	90.21	4.62	92.74	1.53	115.08	1.53
PGD_2	85.04	4.41	97.10	0.98	109.62	2.13
PGE_2	94.22	8.66	92.20	0.74	109.63	2.74
$PGF_2\alpha$	86.21	4.13	92.01	0.80	112.21	2.68
RvD1	86.59	3.25	84.60	1.72	104.69	2.99
RvE1	382.67	16.31	370.75	7.25	191.90	1.41
TXB_2	98.71	4.77	83.93	1.18	101.07	3.57
AA	96.85	15.07	98.72	2.11	111.05	2.66
ALA	76.26	7.09	121.03	3.22	128.08	2.53

DGLA	19.67	/	91.67	4.99	104.61	2.28
DHA	107.96	0.37	69.02	4.96	57.28	5.67
EPA	125.55	2.74	125.82	0.96	134.70	2.11

Table S7: Inter-3-day variability of accuracy and precision/RSD at 0.1, 1 and 10 ng/ml; PUFAs are 10x higher concentrated (n=3)

Metabolites	Accuracy (%)	RSD (%)	Accuracy (%)	RSD (%)	Accuracy (%)	RSD (%)
concentration	0.1 ng/ml		1 ng/ml		10 ng/ml	
±11-HDHA	143.02	30.76	103.49	8.79	103.82	4.95
±11,12-DHET	119.68	1.93	102.83	6.10	100.59	2.20
±12,13-DiHOME	140.53	14.74	102.67	4.62	100.21	1.90
±13-HDHA	180.04	28.11	117.19	13.53	97.64	6.61
±17-HDHA	136.92	15.69	106.39	3.10	101.04	4.52
±18-HEPE	148.14	10.58	110.29	0.99	103.43	5.22
±4-HDHA	202.72	23.32	109.19	23.01	120.00	17.31
±5,6-DHET	141.55	19.66	106.84	4.04	100.89	3.81
±8(9)-DHET	130.38	20.59	106.18	8.78	101.41	5.02
±9-HETE	107.88	10.70	84.90	14.84	87.49	20.97
±9,10-DiHOME	172.42	16.37	116.61	10.92	101.21	7.68
11(12)-EET	142.84	16.30	113.63	2.28	104.05	6.25
11(S)-HETE	144.99	28.43	107.75	6.61	101.55	1.78
12-oxo-ETE	NA	NA	100.58	47.04	90.25	45.12
12(S)-HEPE	166.38	24.39	113.60	3.10	98.01	5.25
12(S)-HETE	230.28	60.98	101.39	1.03	101.57	3.36
13(S)-HODE	166.54	7.11	103.40	6.18	102.73	2.53
14(15)-EET	94.60	15.53	112.79	13.23	101.73	6.35
14(15)-EpETE	140.26	28.50	103.28	9.92	104.94	5.53
15-oxo-ETE	152.39	13.43	113.81	2.28	108.03	6.57
15(S)-HEPE	130.70	9.05	102.36	8.71	101.82	3.17
15(S)-HETE	138.53	16.73	107.79	4.94	111.99	8.42
15(S)-HETrE	138.79	27.16	112.88	8.87	106.01	9.23
15(S)-HpETE	NA	NA	125.99	NA	62.15	86.12
20-HETE	105.16	21.19	104.98	7.27	104.69	1.98
5-oxoETE	128.17	10.70	103.40	10.31	114.85	24.63
5(6)-EET	139.76	23.86	105.50	12.07	91.75	14.08
5(S)-HEPE	149.54	7.15	106.10	2.94	110.07	10.56
5(S)-HETE	231.21	44.70	113.16	7.13	101.12	4.38
5(S)-HpETE	NA	NA	NA	NA	NA	NA
6-keto-$PGF_1\alpha$	102.01	12.82	91.50	6.49	96.75	9.37
8-iso-$PGF_2\alpha$	113.92	9.52	103.22	7.63	103.40	15.29
8(9)-EET	150.18	16.08	111.40	2.65	112.48	9.48
9(S)-HODE	172.33	24.73	105.72	6.30	102.03	4.08
LTB_4	130.61	22.99	107.42	7.22	100.07	2.30
LTC_4	119.86	32.20	101.37	8.37	101.13	3.95
LTD_4	140.30	31.13	107.71	6.63	100.06	3.07
LTE_4	120.35	24.06	109.84	3.07	103.58	5.93
LXA4	134.56	7.52	111.38	5.75	108.98	8.84
MAR1	135.97	21.48	104.56	8.88	102.06	3.55
PDX	130.64	18.81	105.48	13.01	101.45	1.54
PGD_2	131.20	21.28	103.53	7.04	100.79	3.62
PGE_2	125.20	22.41	109.18	5.68	103.26	3.79
$PGF_2\alpha$	147.94	21.55	115.13	4.68	105.34	4.77
RvD1	126.87	20.61	104.69	3.22	101.95	2.58
RvE1	98.36	3.04	98.72	5.59	95.94	14.67
TXB_2	125.13	20.40	104.07	2.74	106.39	7.99
AA	349.17	26.16	120.76	40.71	125.30	25.53
ALA	216.22	55.50	109.50	12.29	96.96	0.97

DGLA	2846.77	134.75	91.21	63.96	68.53	68.78
DHA	10738.50	142.89	1448.42	114.05	118.85	4.64
EPA	296.48	56.65	120.56	44.51	85.10	16.89

Table S8: Limit of detection (LOD) and lower limit of quantitation (LLOQ) with correlation coefficient

Metabolite	LOD (ng/ml)	LLOQ (ng/ml)	Correlation Coefficient
±11-HDHA	0.05	0.5	0.99999
±11,12-DHET	0.005	0.05	0.99999
±12,13-DiHOME	0.005	0.5	0.99993
±13-HDHA	0.1	1	0.99978
±17-HDHA	0.005	1	0.99999
±18-HEPE	0.05	0.5	0.99993
±4-HDHA	0.5	1	1
±5,6-DHET	0.05	0.05	1
±8(9)-DHET	0.005	0.5	0.99992
±9-HETE	0.005	0.5	0.99999
±9,10-DiHOME	0.1	1	0.9999
11(12)-EET	0.005	0.5	0.99999
11(S)-HETE	0.005	0.05	0.99993
12-oxo-ETE	0.5	0.5	0.99977
12(S)-HEPE	0.5	1	0.99998
12(S)-HETE	0.005	1	0.99999
13(S)-HODE	0.1	0.5	0.99999
14(15)-EET	0.01	0.5	0.99989
14(15)-EpETE	0.1	0.5	0.99885
15-oxo-ETE	0.05	0.5	0.99995
15(S)-HEPE	0.05	0.5	0.99992
15(S)-HETE	0.25	0.05	0.99994
15(S)-HETrE	0.1	10	0.99984
15(S)-HpETE	0.005	NA	0.99958
20-HETE	0.01	1	0.99946
5-oxoETE	0.005	0.05	0.99992
5(6)-EET	0.01	NA	0.99955
5(S)-HEPE	0.05	0.05	0.99999
5(S)-HETE	0.5	0.05	1
5(S)-HpETE	NA	NA	N/A
6-keto-$PGF_1\alpha$	0.01	0.1	0.99958
8-iso-$PGF_2\alpha$	0.005	0.5	0.99951
8(9)-EET	0.05	0.1	0.99994
9(S)-HODE	0.1	0.05	0.99998
LTB_4	0.005	0.05	0.99998
LTC_4	0.005	0.005	0.99959
LTD_4	0.005	0.5	0.99988
LTE_4	0.005	0.5	0.99998
LXA4	0.005	0.5	0.99996
MAR1	0.005	1	0.99988
PDX	0.005	0.5	0.99945
PGD_2	0.005	0.5	0.99975
PGE_2	0.005	0.5	0.99947
$PGF_2\alpha$	0.005	0.5	0.99995
RvD1	0.005	0.5	0.99999
RvE1	0.05	0.05	0.99999
TXB_2	0.005	0.25	0.99996
AA	500	100	0.99948
ALA	50	100	0.9995
DGLA	50	1	0.99986
DHA	500	NA	0.99568
EPA	50	100	0.99911

Table S9: Comparison of Frankfurt and Munich LC-MS/MS panels, data are shown as mean ± SD for 6 different blood donors.

Metabolite	Frankfurt (ng/ml) (method 2)	Munich (ng/ml) (method 1)
PGD_2	0.009 ± 0.005	0.012 ± 0.008
PGE_2	0.012 ± 0.012	0.008 ± 0.007
$PGF_2\alpha$	0.018 ± 0.017	0.050 ± 0.065
LTB_4	9.061 ± 4.342	29.097 ± 34.562
TXB_2	0.298 ± 0.380	0.186 ± 0.210
5-HETE	8.411 ± 9.181	11.913 ± 12.668
15-HETE	0.237 ± 0.547	0.110 ± 0.066